Cell Research (2017) 27:1046-1064.

www.nature.com/cr

ORIGINAL ARTICLE

Existing drugs as broad-spectrum and potent inhibitors for Zika virus by targeting NS2B-NS3 interaction

Zhong Li[1, *], Matthew Brecher[1, *], Yong-Qiang Deng[2, *], Jing Zhang[1], Srilatha Sakamuru[3], Binbin Liu[1, 4], Ruili Huang[3], Cheri A Koetzner[1], Christina A Allen[5], Susan A Jones[1], Haiying Chen[6], Na-Na Zhang[2], Min Tian[2], Fengshan Gao[1, 7], Qishan Lin[8], Nilesh Banavali[1, 9], Jia Zhou[6], Nathan Boles[5], Menghang Xia[3], Laura D Kramer[1, 9], Cheng-Feng Qin[2, 10], Hongmin Li[1, 9]

[1]Wadsworth Center, New York State Department of Health, 120 New Scotland Ave, Albany, NY 12208, USA; [2]Department of Virology, State Key Laboratory of Pathogen and Biosecurity, Beijing Institute of Microbiology and Epidemiology, Beijing 100071, China; [3]National Center for Advancing Translational Sciences, National Institutes of Health, Bethesda, MD 20892, USA; [4]Department of Food Science, College of Food Science and Technology, Guangdong Ocean University, Zhanjiang, Guangdong 524000, China; [5]The Neural Stem Cell Institute, 1 Discovery Drive, Rensselaer, NY 12144, USA; [6] Department of Pharmacology and Toxicology, Chemical Biology Program, University of Texas Medical Branch, Galveston, TX 77555, USA; [7]Department of Biochemistry and Molecular Biology, College of Life Science and Technology, Dalian University, Dalian, Liaoning 116622, China; [8]Center for Functional Genomics, University at Albany, Rensselaer, NY 12144, USA; [9]Department of Biomedical Sciences, School of Public Health, University at Albany, PO Box 509, Empire State Plaza, Albany, NY 12201, USA; [10]Guangzhou Eighth People's Hospital, Guangzhou Medical University, Guangzhou, Guangdong 510060, China

Recent outbreaks of Zika virus (ZIKV) highlight an urgent need for therapeutics. The protease complex NS2B-NS3 plays essential roles during flaviviral polyprotein processing, and thus represents an attractive drug target. Here, we developed a split luciferase complementation-based high-throughput screening assay to identify orthosteric inhibitors that directly target flavivirus NS2B-NS3 interactions. By screening a total of 2 816 approved and investigational drugs, we identified three potent candidates, temoporfin, niclosamide, and nitazoxanide, as flavivirus NS2B-NS3 interaction inhibitors with nanomolar potencies. Significantly, the most potent compound, temoporfin, not only inhibited ZIKV replication in human placental and neural progenitor cells, but also prevented ZIKV-induced viremia and mortality in mouse models. Structural docking suggests that temoporfin potentially binds NS3 pockets that hold critical NS2B residues, thus inhibiting flaviviral polyprotein processing in a non-competitive manner. As these drugs have already been approved for clinical use in other indications either in the USA or other countries, they represent promising and easily developed therapies for the management of infections by ZIKV and other flaviviruses.

***Keywords*:** Zika virus; inhibitor; protease; NS2B-NS3

Cell Research (2017) **27**:1046-1064. doi:10.1038/cr.2017.88; published online 7 July 2017

Introduction

The genus *Flavivirus* is composed of more than 70 viruses, many of which cause severe human diseases with global impact, e.g., dengue viruses (DENV), yellow fever virus (YFV), West Nile virus (WNV), and Japanese encephalitis virus (JEV). Significant outbreaks of ZIKV, a re-emerging mosquito-borne flavivirus, have occurred worldwide since 2013 [1, 2]. Importantly, ZIKV infection has led to a global crisis due to its unexpected links to testis damage [3, 4], ocular damage [5, 6], Guillain-Barre syndrome, fetal microcephaly [1, 7-9], and potentially to other neural complications [10-12].

Like other flavivirus members, the ZIKV genome is ~11 kb in length, consisting of a 5′ UTR, a single long

*These three authors contributed equally to this work.
Correspondence: Cheng-Feng Qin[a], Hongmin Li[b]
[a]Tel: +86-10-66948604
E-mail: qincf@bmi.ac.cn
[b]Tel: +1 518 4734201
E-mail: Hongmin.li@health.ny.gov
Received 4 February 2017; revised 19 May 2017; accepted 5 June 2017; published online 7 July 2017

open reading frame (ORF), and a 3′ UTR. The single ORF encodes a polyprotein precursor (PP) that is further processed into three structural proteins (C, prM, and E) and seven non-structural proteins. Among these viral proteins, NS3 is a protein with multiple functions, including protease activity. The flaviviral protease, which works together with host proteases to cleave the viral PP, is a highly conserved enzyme essential for replication [13, 14]. The viral protease is a complex of two components, NS2B and NS3. NS2B is an essential cofactor for NS3 protease function [15, 16].

The NS2B-NS3 protease is a high-priority drug target [17-20]. Most attempts to develop flavivirus protease inhibitors have focused on the NS3 active site with limited success, possibly due to two of the site's features (reviewed in [21-24]). First, the active site is flat and featureless, which making it difficult to design specific and potent inhibitors. Second, because the active site preferentially binds substrates with charged residues in the P1 and P2 sites, active site inhibitors effective in biochemical assays are similarly charged and consequently show poor bioavailability *in vivo*.

Unlike the flat and featureless active site, the NS3 pockets holding the NS2B N-terminal residues (such as key contact residues L51, L53, V59, and W61, DENV2 number) are deep and hydrophobic. Because the NS2B binding is essential for protease function, we investigated whether we could develop an alternative strategy to target the NS2B-NS3 interaction interface to orthosterically inhibit the NS3 protease function. In this way we sought a novel approach to avoid the active site's featureless nature and the necessity for strongly charged inhibitors.

To test this approach, we developed a novel split luciferase complementation (SLC)-based high-throughput screening (HTS) assay to identify orthosteric inhibitors capable of abolishing the NS2B-NS3 interactions. We screened the NIH Chemical Genomic Center (NCGC) Pharmaceutical Collection library, which contains 2 816 approved and investigational drugs. Three approved compounds were identified that broadly inhibited flaviviruses at nanomolar efficacy. The most potent drug, temoporfin, not only inhibited ZIKV infection in human placental and neural progenitor cells, but also prevented ZIKV-induced viremia and mortality in mouse models. Our findings suggest potential for a rapid resolution of the urgent need for a potent anti-ZIKV drug.

Results

Development of SLC-based NS2B-NS3 interaction assay

To explore whether orthosteric inhibitors abolishing the NS2B-NS3 interactions could inhibit the NS3 protease function, we developed a SLC-based NS2B-NS3 interaction assay (Figure 1A and Supplementary information, Figure S1). We constructed, expressed, and purified several fusion proteins, including Nluc416 (aa 1-416 of FLuc)-NS2B (named Nluc-NS2B), GST-NS3-Cluc398 (aa 398-550 of FLuc, named GNC), NS2B-NLuc, GST-Cluc-NS3 (named GCN), Nluc-NS2B aa 49-66 (named Nluc-E66stop), and NS2B aa 49-66-Nluc (named E66stop-Nluc). We first checked that none of these constructs individually produced any luminescence (Figure 1B). Our data also confirm that the positions of luciferase fragments are important (Figure 1B), as signals for GCN paired with any NLuc-NS2B fragment construct (black) are much stronger than those for GNC counter pairs (grey). Among these pairs, NLuc-E66stop/GCN produced the strongest signal. Therefore, we chose this pair to perform all the following experiments in an assay optimized by varying the detergent that was used (Figure 1C) and the concentration of Nluc-E66stop and GCN (optimal with each at 100 nM). In addition, when the Nluc-E66stop was fixed at a very low concentration (10 nM), we could observe the dose-dependent SLC signal as GCN varied in concentration.

SLC specificity and affinity determination

Specificity of the assay is an important factor for any HTS approach. To confirm this, we first used "cold" MBP-NS3 as a competitor against GCN in our SLC-based NS2B-NS3 interaction assay. MBP-NS3 greatly reduced the SLC signals from the NLuc-E66stop/GCN interactions, whereas the maltose-binding protein (MBP) fusion tag did not show any inhibition (Figure 1E). The reaction was dose-dependent with an affinity of 2.5 μM (Figure 1F). Moreover, mutations of the NS2B residues L51, L53, and V59, known to be essential for protease function [15], significantly reduced the SLC (Figure 1G). Together, the results indicate that the SLC signal from NLuc-E66stop/GCN pair is specific to the interactions between NS2B and NS3.

SLC assay with a known orthosteric inhibitor

It was previously reported that the small molecule SK-12 is an orthosteric inhibitor blocking NS2B-NS3 interactions [25]. Mutagenesis studies indicate that SK-12 interacts with the DENV NS3 residue at position 27, which is part of the pocket holding the NS2B residue L51[25]. We first verified that SK-12 inhibited the SLC in a dose-dependent manner with an $IC_{50\text{-SLC}}$ of 10 μM (Figure 2A); at 40 μM SK-12 gave significant and robust inhibition of the SLC of NLuc-E66-stop/GCN with a signal/background (S/B) ratio (DMSO vs SK-12) of 8.4-fold (Figure 2B). The *Z*-score of 0.83 is better than the

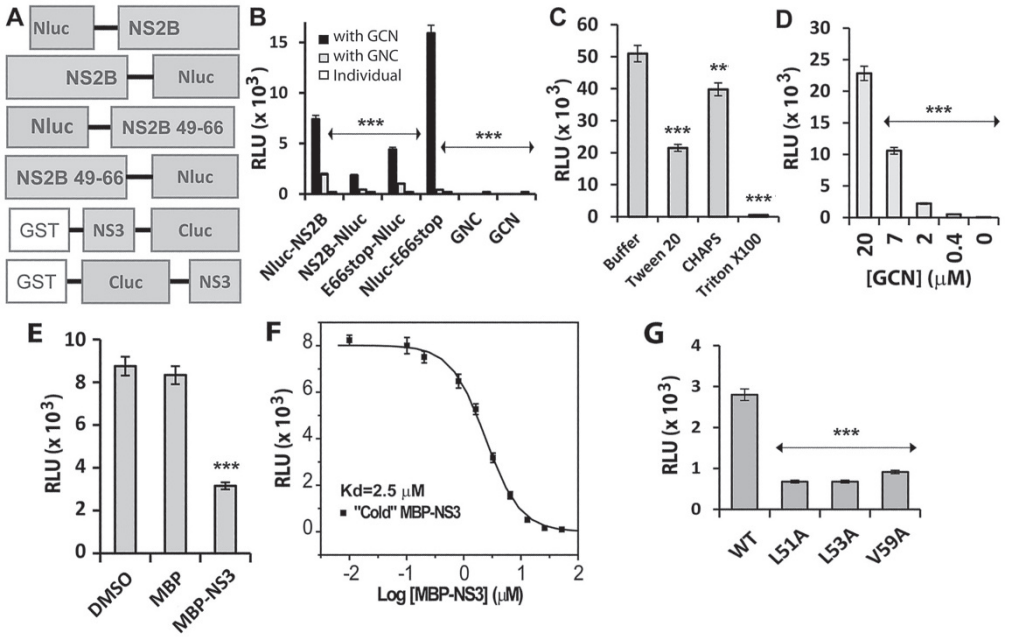

Figure 1 The DENV2 NS2B/NS3 SLC assays. **(A)** The DENV2 NS2B/NS3 SLC constructs. NLuc aa 1-416-NS2B (named as NLuc-NS2B), NS2B-NLuc aa 1-416 (NS2B-NLuc), NLuc416-NS2B aa 49-66 (NLuc-E66stop), NS2B (aa 49-66)-NLuc416 (E66stop-NLuc), GST-NS3-CLuc aa 398-550 (GNC), and GST-CLuc (aa 398-550)-NS3 (GCN). **(B)** The positions of NLuc and CLuc are important. Equal concentrations (100 nM) of each pair of NS2B/NS3 constructs were mixed (or alone) and incubated with luciferin substrate. ***P < 0.001. In all bar graphs, means and SD from triplicate experimental data were shown, unless otherwise specified. **(C)** Effects of detergent at 0.05% concentration. **P < 0.01; ***P < 0.001. **(D)** Dose-response of NLuc-E66stop/GCN pair. Nluc-E66stop at 20 nM was included in each experiment. Concentration of GCN was varied as indicated. ***P < 0.001. **(E)** The DENV2 MBP-NS3 fusion protein specifically inhibited the SLC by NLuc-E66stop and GCN (80 nM each). MBP-NS3 or MBP were at 3.25 μM each. ***P < 0.001. **(F)** Dose-response inhibition of the SLC signals from NLuc-E66stop and GCN by "cold" MBP-NS3. Experimental data were fitted using the sigmoidal function with the Origin6.0 software. **(G)** NS2B mutations greatly reduced SLC. GCN was paired with equal molar of NLuc-E66stop or NLuc-E66stop mutants (L51A, L53A, and V59A). ***P < 0.001.

gold standard (Z-score of 0.5) for an HTS assay (Figure 2B). More importantly, when NLuc-E66stop and GCN were co-expressed in *Escherichia coli* cells, addition of SK-12 significantly suppressed the SLC signal (Figure 2C). These data suggested that even though NS2B and NS3 are expressed together in cells, the NS3 pockets for NS2B binding remain accessible to small molecule inhibitors. These results indicate that the SLC HTS assay offers a promising strategy for screening compounds to interfere with NS2B-NS3 interactions.

Identification of existing drugs as inhibitors of NS2B-NS3 interaction using qHTS

The SLC assay was successfully transferred from the 96-well plate to a 1 536-well plate format allowing us to perform a quantitative HTS (qHTS) screen against the NIH NCGC Pharmaceutical Collection [26]. The qHTS assay was of high quality with an averaged S/B ratio of 8.1 ± 1.5 and a Z'-score of 0.66 ± 0.03 for all 20 plates (Figure 2D). Twenty-three compounds were confirmed to have $IC_{50\text{-SLC}}$ values < 15 μM. Eleven compounds that might be *pan assay interference compounds* (PAINS) [27] were removed after examination of their chemical structures. The remaining 12 compounds were subjected to further studies.

Characterization of drugs on protease inhibition

To characterize protease inhibition activities, we expressed and purified His-tagged NS2B and the DENV2 NS3 protease domain fused to MBP (Figure 2E, Supplementary information, Figure S2A and S2B). We also generated a cleavable MBP-NS3 by engineering a thrombin cleavage site between MBP and NS3. Our results show that addition of the MBP tag greatly enhances the solubility of NS3, allowing purification of soluble MBP-NS3 directly from the cleared supernatant of a cell lysate. However, upon removal of the MBP tag by thrombin digestion, the majority of the cleaved NS3 protease domain

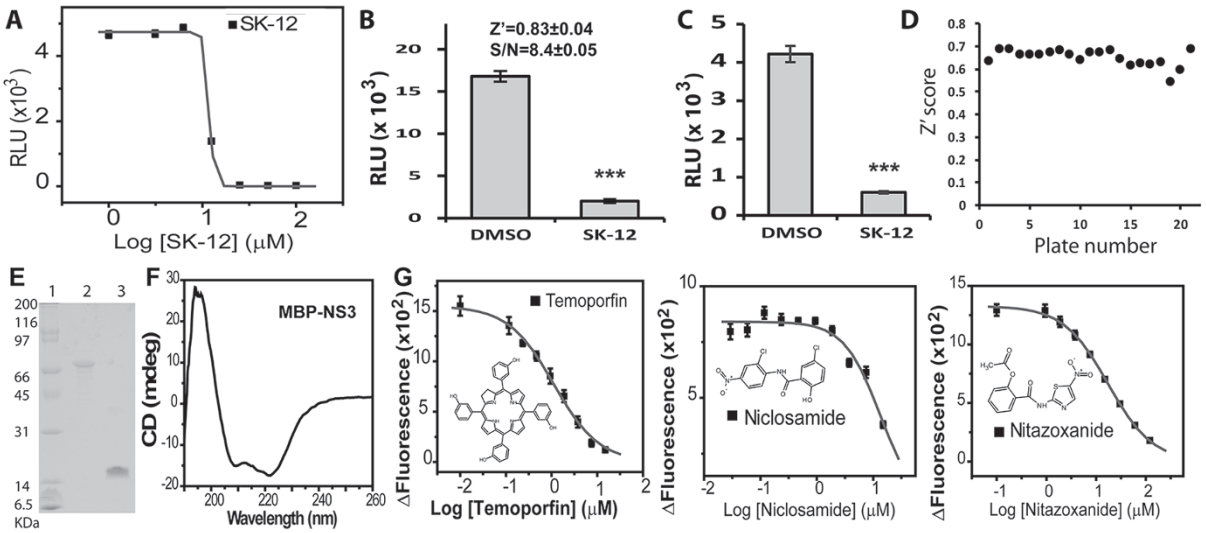

Figure 2 HTS assay identified potent orthosteric protease inhibitors. **(A)** Dose-response inhibition of the SLC signals from NLuc-E66stop and GCN by SK-12. Experimental data were fitted using the sigmoidal function with the Origin6.0 software. **(B)** HTS parameters using purified NLuc-E66stop and GCN. NLuc-E66stop and GCN at 100 nM were used with DMSO or SK-12 (40 μM). n = 8. ***P < 0.001. **(C)** NS3 pockets were accessible to small molecule inhibitor when NS2B and NS3 were co-expressed. Plasmids of NLuc-E66stop and GCN were co-transformed into *Escherichia coli* BL21 (DE3). Cells were grown to OD_{600} of 0.6 and were induced by IPTG. Cells were continuously grown for 2 h, collected and resuspended in luciferase assay buffer. About 100 μl of cells was dispensed into a 96-well plate, incubated with 1% DMSO or SK-12 (40 μM) for 2 h, then mixed with substrate luciferin n = 8. ***P < 0.001. **(D)** Summary of HT screening of the NCGC Pharmaceutical Collection in all plates. Statistics were generated by averaging those of 20 plates that were calculated from 32 wells in each plate. **(E)** SDS-PAGE analysis of purified His-MBP-NS3 (lane 2) and His-NS2B (Lane 3). Lane 1, Bio-Rad broad range molecular weight (MW) standard. **(F)** CD spectrum of purified His-MBP-NS3. **(G)** Sigmoidal curve fittings of dose-response inhibitions of the His-NS2B/His-MBP-NS3 protease activities by drugs. Inset: schematic representations of identified drugs.

precipitated. These results are consistent with the fact that in the absence of the NS2B cofactor, NS3 is insoluble and requires *in vitro* refolding [28, 29]. Circular dichroism (CD) analysis indicated that purified MBP-NS3 was correctly folded, displaying a typical CD spectrum of an αβ protein (Figure 2F).

In order to compare the activity of the MBP-NS3 fusion protein and native NS3, we generated and refolded a His-tagged NS3 protease domain, as described previously (Supplementary information, Figure S2C) [28, 29]. We found that both soluble MBP-NS3 fusion protein and refolded NS3 can be trans-activated by soluble His-NS2B, and have similar activities (Supplementary information, Figure S2D). Therefore, all subsequent experiments for protease activity were based on the MBP-NS3 fusion protein.

Using a protease inhibition assay, we tested whether the 12 drugs identified could inhibit the protease activity of the MBP-NS3 and His-NS2B heterocomplex. Our results showed that three compounds, namely temoporfin, niclosamide, and nitazoxanide, effectively inhibited the NS2B-NS3 protease activity with $IC_{50\text{-pro}}$ values ranging from 1.1 to 15.9 μM (Table 1 and Figure 2G).

Identification of drugs as potent anti-ZIKV inhibitors

A virus plaque reduction assay with DENV2 showed that infectious virus production was significantly reduced in the presence of the three identified drugs at concentrations of 2 μM (temoporfin and niclosamide) or 10 μM (all three drugs) **(**Figure 3A). A cell viability assay was then performed to investigate whether some of this reduction in viral titer could be the result of compound cytotoxicity (Figure 3B). With the exception of niclosamide, which displays cytotoxicity with a CC_{50} of 4.8 μM, the other two drugs have minimal cytotoxicity on A549 cells (Figure 3B and Table 1). Thus the antiviral effects of these compounds are not attributable to cytotoxicity.

Because there is currently an urgent need for a ZIKV treatment and as the compounds we identified are likely to be broad-spectrum inhibitors, we tested their antiviral efficacy against ZIKV using the Puerto Rico strain PRVABC59 (Figure 3C and Table 1). Our data indicate that temoporfin is a very potent ZIKV inhibitor with an EC_{50} in a low nanomolar range (24 nM). Further tests with an-

Table 1 Protease inhibition, cytotoxicity, and broad-spectrum anti-flavivirus activities

Compound	$IC_{50\text{-pro}}^{\neq}$ (μM)	$CC_{50}^{\neq}$ (μM)	Virus	$EC_{50}^{\neq}$ (μM)	$EC_{90}^{\neq}$ (μM)	TI#
temoporfin	1.1 ± 0.1	40.7 ± 0.7	ZIKV	0.024 ± 0.003	0.13	1 696
			ZIKV*	0.022 ± 0.002	0.12	1 850
			DENV2	0.020 ± 0.003	0.11	2 035
			WNV*	0.010 ± 0.001	0.030	4 070
			JEV*	0.011 ± 0.001	0.025	3 700
			YFV*	0.006 ± 0.001	0.015	6 783
niclosamide	12.3 ± 0.6	4.8 ± 1.0	ZIKV	0.48 ± 0.06	1.9	10
			DENV2	0.55 ± 0.05	2.3	9
			WNV	0.54 ± 0.17	2.3	9
			JEV	1.02 ± 0.08	2.4	3.8
			YFV	0.84 ± 0.02	1.9	5.7
nitazoxanide	15.9 ± 0.9	77 ± 7.2	ZIKV	1.48 ± 0.18	4.0	52
		60 [54]	JEV	0.39 [54]		154 [54]

*Experiment was performed without ambient light (in dark).

$IC_{50\text{-pro}}^{\neq}$, compound concentration required to inhibit 50% of a reaction or binding; $CC_{50}^{\neq}$: the concentration of compound at which 50% cells are viable; $EC_{50}^{\neq}$ and $EC_{90}^{\neq}$: the effective concentration of a drug at which virus production is reduced by 50% or 90%, respectively. TI#, therapeutic index defined as CC_{50}/EC_{50}.

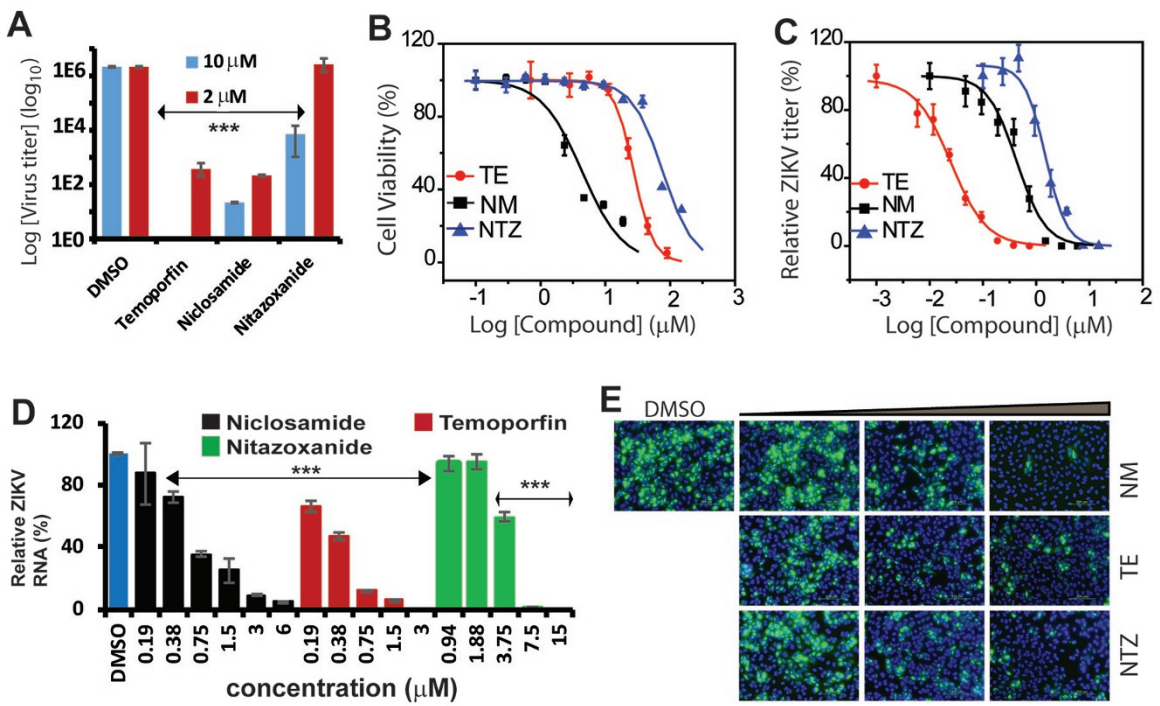

Figure 3 Drugs are potent inhibitors of ZIKV and DENV2. **(A)** Inhibition of DENV2 in viral reduction assay in A549 cells by temoporfin (TE), niclosamide (NM), and nitazoxanide (NTZ) at 10 and 2 μM concentrations. ***P < 0.001. **(B)** Cell viability assay. A549 cells were incubated with various concentrations of drugs and then assayed for viability at 48 h post incubation. Experimental data were fitted using a sigmoidal function. **(C)** Sigmoidal fittings of dose-dependent inhibition of ZIKV by drugs in A549 cells. Viral plaque reduction assay was used. **(D)** qRT-PCR analysis of inhibition of viral RNA from ZIKV-infected A549 cells by drugs. ***P < 0.001. **(E)** Immunofluorescence assay of inhibition of viral protein expression by drugs, using pan-flavivirus anti-E 4G2 antibody (green) (ATCC). Concentration for drugs: (1) niclosamide: 0.19, 0.57, and 1.67 μM; (2) temoporfin: 0.06, 0.56, and 5 μM; (3) nitazoxanide: 0.06, 0.56, and 5 μM; Nuclei (blue) were stained in all immunofluorescence assays (IFA) by the Hoechst stain solution.

other Venezuela strain GZ01 also showed a similar result for temoporfin (Supplementary information, Figure S3). Niclosamide and nitazoxanide are also very potent ZIKV inhibitors with EC_{50} values in low micromolar range. With the exception of niclosamide, the EC_{50} values for two other drugs are well below cytotoxic concentrations, with therapeutic indexes well above the threshold of 10 (Table 1).

Although it can be photosensitized [30, 31], temoporfin significantly reduced the titer of ZIKV in the absence of light exposure for all viruses tested (Table 1). Thus temoporfin does not require photoactivation to inhibit the virus titer.

To further characterize the three inhibitors, we performed quantitative real-time PCR (qRT-PCR) and immunofluorescence assays (Figure 3D and 3E). Additions of these drugs greatly reduced both viral RNA copy numbers and viral antigen expression in a dose-dependent manner.

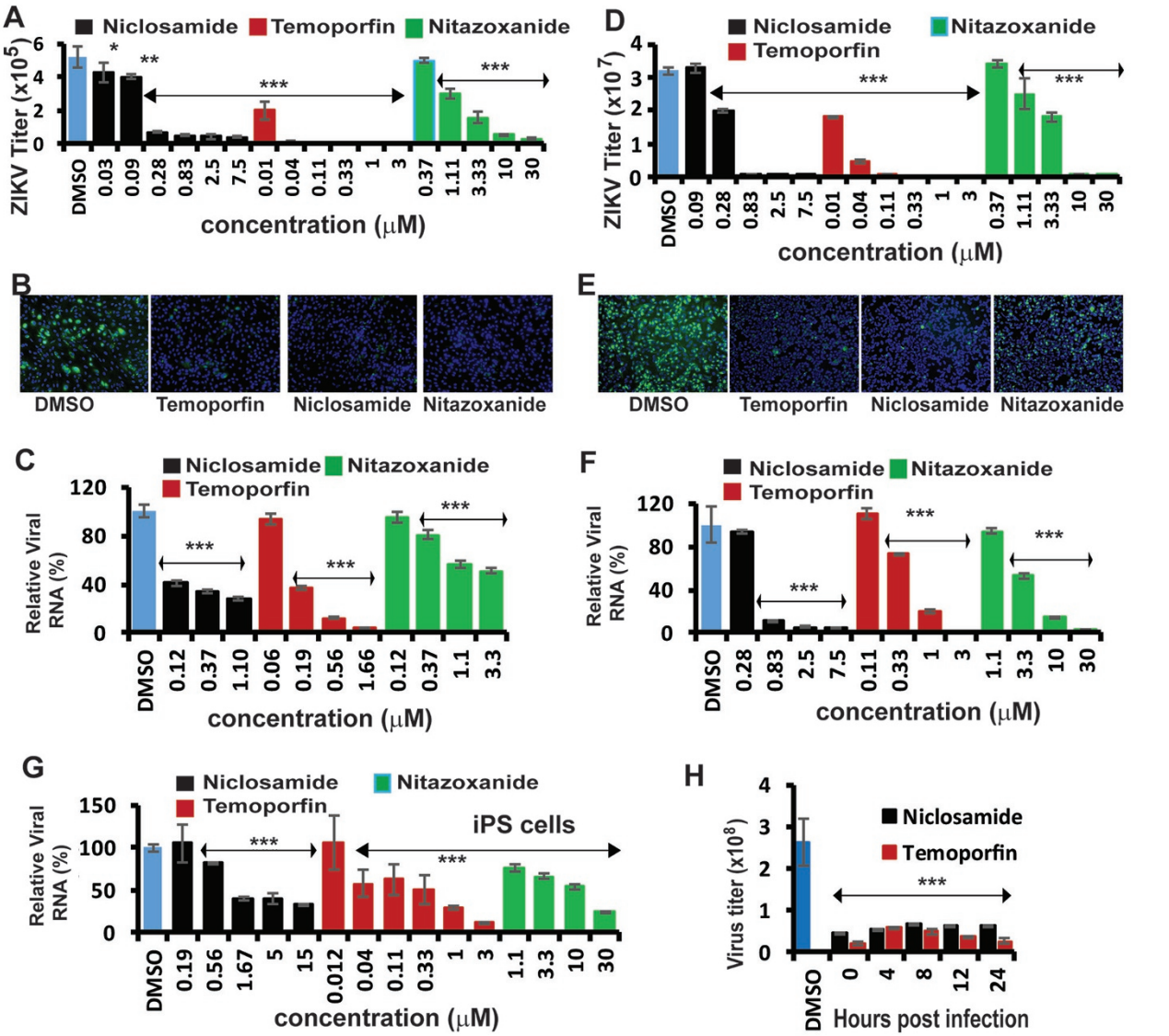

Figure 4 Inhibition of ZIKV in cells relevant to ZIKV. **(A**, **D)** Viral plaque reduction assay for ZIKV-infected HPECs **(A)** and iPSC-derived hNPCs **(D)** by drugs. **P* < 0.05; ***P* < 0.01; ****P* < 0.001. **(B**, **E)** Immunofluorescence assays (IFA) of inhibition of viral protein expression for ZIKV-infected HPECs **(B)** and hNPCs **(E)** by drugs. For HPECs, temoporfin (0.06 μM), niclosamide (0.19 μM), and nitazoxanide (10 μM). For hNPCs, temoporfin (1.0 μM), niclosamide (0.83 μM), and nitazoxanide (3.3 μM). **(C**, **F)** qRT-PCR analysis of inhibition of viral RNA of ZIKV-infected HPECs **(C)** and hNPCs **(F)** by drugs. ****P* < 0.001. **(G)** qRT-PCR analysis of inhibition of viral RNA of ZIKV-infected iPSC HDF9 by drugs. ****P* < 0.001. **(H)** Time-of-addition study of ZIKV inhibition in A549 cells by temoporfin (90 nM) and niclosamide (0.75 μM). ****P* < 0.001.

Inhibition of ZIKV in human placental epithelial cells

ZIKV causes microcephaly in newborns after infecting fetal and placenta cells during pregnancy [32]. To investigate antiviral efficacy in this context, we tested the ability of these compounds to inhibit ZIKV in human placental epithelial cells (HPECs) that are derived from the inner surface of the amnion and have physiology relevant to fetal development and neurogenesis. All three drugs effectively inhibited ZIKV in HPECs (Figure 4A) and drastically decreased protein expression and viral RNA replication (Figure 4B and 4C). Together, these experiments demonstrate the compounds to be effective antivirals in placental cells relevant to ZIKV infection.

Inhibition of ZIKV in human stem cells and neural progenitor cells

As ZIKV also targets human neuronal progenitor cells (hNPCs) and neurons [33-36], we further evaluated drug efficacy in the human induced pluripotent stem cell (iPSC) line HDF9 [37] and iPSC-derived hNPCs [38]. We found that all three drugs considerably reduced ZIKV titers in hNPCs and HDF9 iPSCs (Figure 4D-4G). These results confirm the likely efficacy of these compounds for controlling ZIKV infection in these types of cells.

Inhibition of ZIKV post infection

To test the ability of the compounds to control existing infections, we tested the effects of adding the two most potent drugs, temoporfin and niclosamide (Figure 4H) 24-h post infection (pi). We found these treatments were almost equally effective as additions at the time of infection, implying that temoporfin and niclosamide are potent inhibitors for ZIKV not only during the early stages of viral infection, but also in the late stages of viral replication.

Broad antiviral spectrum

Inhibitors targeted to the NS2B-binding site on NS3 may have broad-spectrum anti-flaviviral activity, as this site is conserved among flavivirus NS3 proteases. In support of this idea, we also tested the ability of temoporfin and niclosamide to inhibit DENV2, WNV, JEV, and YFV infection. Our results clearly demonstrate that both temoporfin and niclosamide are broad-spectrum inhibitors against all flaviviruses tested in addition to ZIKV, and exhibit similar potencies (Table 1).

In vivo protection of mice from lethal challenge of ZIKV

Because temoporfin has a nanomolar anti-ZIKV potency, we evaluated the *in vivo* anti-ZIKV potential of temoporfin using mouse models. In the viremia model [39, 40], temoporfin treatment resulted in about 100-fold reduction in ZIKV-induced viremia in immunocompetent Balb/C mice compared to the vehicle control (Figure 5A). In the lethal A129 mouse model [41, 42], all the ZIKV-infected animals treated with vehicle died with typical neurological symptoms including hind limb weakness and paralysis. Significantly, treatment with 1 mg/kg temoporfin for 5 days protected 83% of the infected animals (Figure 5B). None of the surviving mice showed any neurological signs.

In vitro inhibition of NS2B binding to NS3

In order to investigate whether the compounds interfered with the NS2B - NS3 interaction, we first generated GST-tagged ZIKV GST-NS3 protease domain and FLAG-tagged ZIKV NS2B cofactor. We then performed competitive GST pull-down assay using immobilized GST-NS3 and FLAG-tagged NS2B. We verified that FLAG-tagged NS2B could be specifically pulled down by GST-NS3 but not by the GST tag (Figure 6A). We then demonstrated that pre-incubation of the identified

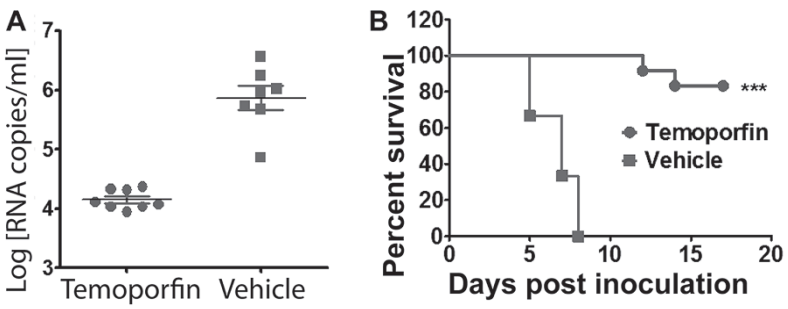

Figure 5 *In vivo* antiviral activity of temoporfin against ZIKV. **(A)** Viremia was detected by RT-qPCR on day 2 post-ZIKV infection in 3-week-old Balb/C mice. Difference between temoporfin (n = 8) or vehicle (n = 7) treatment was analyzed by using the unpaired, two-tailed t-test. **(B)** Survival percentage for 4-week-old A129 mice infected with ZIKV and treated with temoporfin (n = 12) or vehicle (n = 10). Survival curves were compared using the Log-rank test.

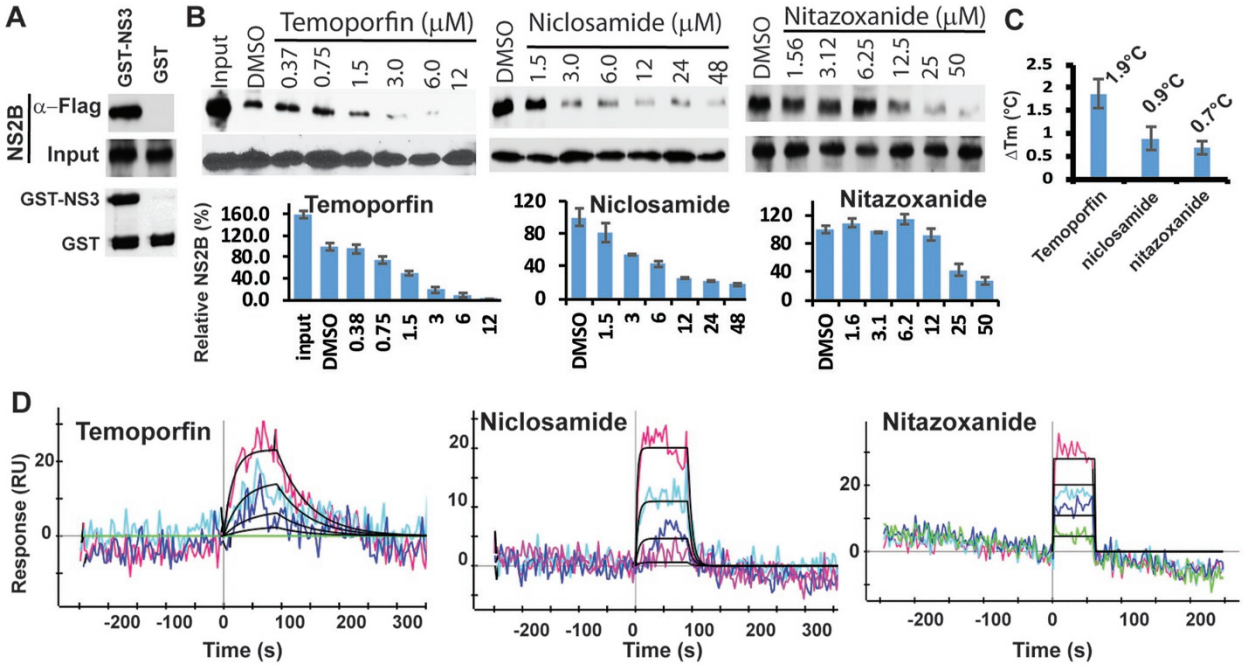

Figure 6 Drugs directly bind to the NS3 protease domain and disrupt interactions between NS2B and NS3. **(A)** GST pull-down assay. GST-NS3 or the GST-tag (10 μg) was immobilized on the Glutathione sepharose-4B affinity beads (GE HealthCare). The FLAG-tagged NS2B (10 μg) was incubated with the beads for 2 h, and subjected to western blots (WB), using anti-FLAG (Genscript) and anti-GST antibodies (GE HealthCare). **(B)** Dose-dependent inhibition of NS2B-NS3 interactions by drugs, using the GST pull-down assay. The assay was performed the same as in **A**, except that two-fold dilution series of drugs were incubated with the GST-NS3 beads overnight prior to incubation with the FLAG-NS2B. Bottom panels showed normalized binding of FLAG-tag NS2B to GST-NS3. The binding of NS2B to NS3 in the absence of each drug (DMSO control) was set as 100%. The relative binding of NS2B to NS3 in the presence of each drug was normalized to the DMSO control. n = 3. **(C)** PTSA for binding of drugs to the MBP-NS3 protein. ΔT_m was defined as $T_{m-drug} - T_{mDMSO}$. **(D)** SPR sensorgrams of kinetic data for the binding of drugs to refolded NS3. The refolded His-NS3 was coupled to a ProteOn GLH sensor chip (~15 000 RU). Each drug with three-fold dilutions was injected. Global fitting of data to a 1:1 binding model is shown in dark black.

drugs with immobilized GST-NS3 beads significantly decreased the binding of the FLAG-NS2B to the GST-NS3, and did so in a dose-dependent manner (Figure 6B). The results indicate that temoporfin, niclosamide, and nitazoxanide each specifically disrupt the interactions between the viral NS2B co-factor and the NS3 protease domain *in vitro*.

Binding of drugs to the NS3 protease domain

We next performed protein thermal shift assays (PTSA) to investigate binding of these compounds to NS3. In these assays, treatment with temoporfin, niclosamide, or nitazoxanide led to increased T_m for purified DENV2 MBP-NS3 protein, compared to the DMSO control (Figure 6C). These data indicate that all three drugs bind to the NS3 protein, resulting in stabilization of the NS3 conformation and leading to T_m increase.

To further investigate whether the drugs could bind to the NS3 protease domain, we used the surface plasmon resonance (SPR) to determine the binding affinity between the identified drugs and the refolded NS3 protease domain (Figure 6D). The drugs bound to the NS3 protease domain with low micromolar affinity, in the order temoporfin (0.4 μM) > niclosamide (6.4 μM) > nitazoxanide (7.3 μM).

Our determinations of T_m and binding affinity accord with each other and with our protease inhibition data. Among the three compounds, the T_m increase for the temoporfin-treated sample was the largest, indicating that temoporfin binds NS3 the strongest. Temoporfin was also the most potent NS2B-NS3 inhibitor and had the highest binding affinity to NS3. In contrast, nitazoxanide led to the smallest T_m increase, consistent with it being the weakest NS2B-NS3 protease inhibitor and exhibiting the lowest binding affinity to NS3.

Non-competitive inhibition of the NS2B-NS3 protease

To further determine the inhibition mechanism, we

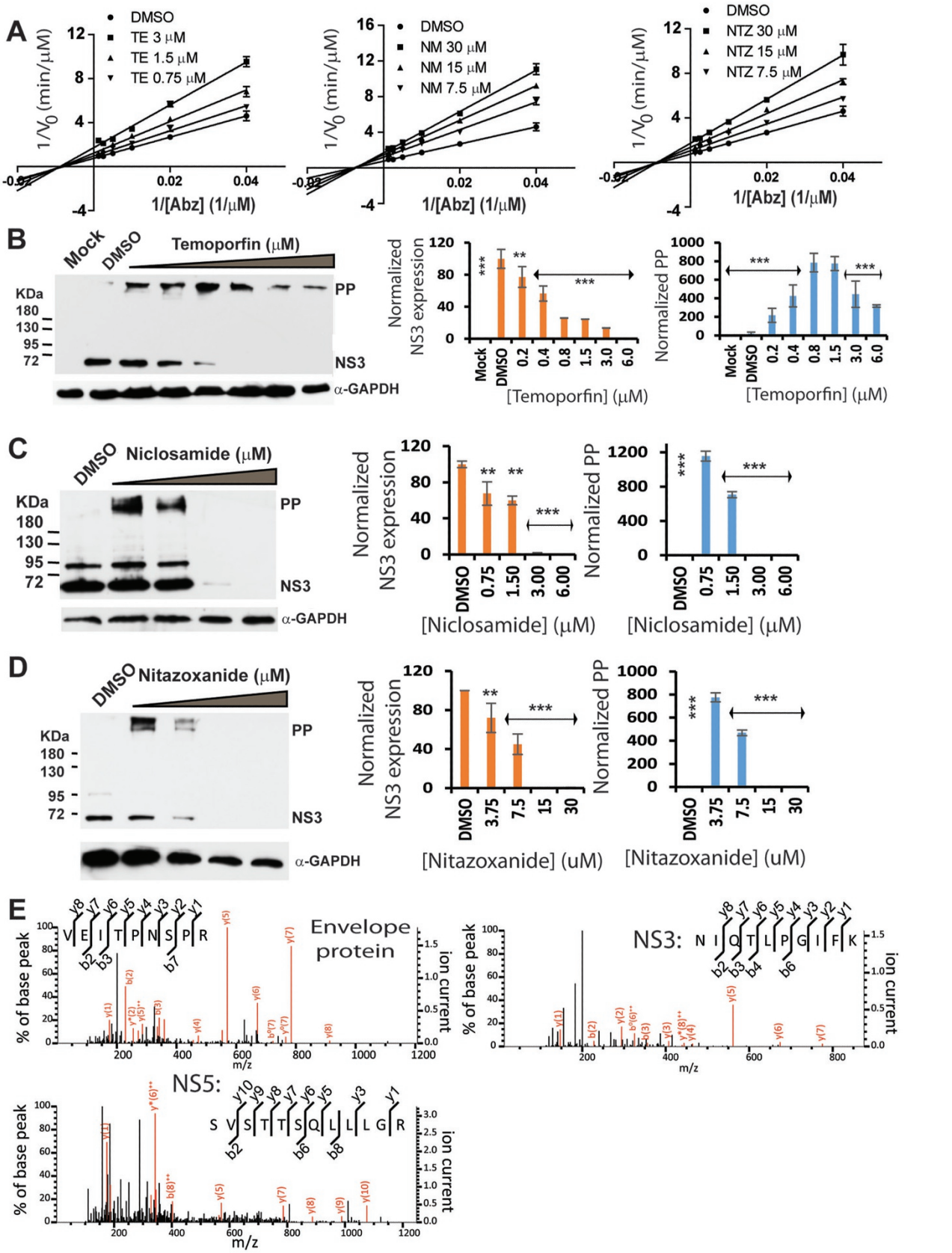
A
DMSO
TE 3 μM
TE 1.5 μM
TE 0.75 μM
1/V0 (min/μM)
1/[Abz] (1/μM)
DMSO
NM 30 μM
NM 15 μM
NM 7.5 μM
DMSO
NTZ 30 μM
NTZ 15 μM
NTZ 7.5 μM
B
Mock
DMSO
Temoporfin (μM)
KDa
180
130
95
72
PP
NS3
α-GAPDH
Normalized NS3 expression
Normalized PP
[Temoporfin] (μM)
C
DMSO
Niclosamide (μM)
[Niclosamide] (μM)
D
Nitazoxanide (μM)
[Nitazoxanide] (uM)
E
Envelope protein
V E I T P N S P R
NS3:
N I Q T L P G I F K
NS5:
S V S T T S Q L L L G R
% of base peak
ion current
m/z

Figure 7 Drugs inhibit viral polyprotein precursor (PP) processing. **(A)** Lineweaver-Burk plot of kinetics experimental data for inhibition of the His-NS2B/His-MBP-NS3 protease complex by drugs. The DENV2 MBP-NS3 (100 nM) was mixed with temoporfin (3, 1.5, and 0.75 μM), niclosamide (30, 15, and 7.5 μM), or nitazoxanide (30, 15, and 7.5 μM) for 30 min. The DENV2 His-NS2B (1 μM) was added together with the Abz substrate at various concentrations (800-25 μM in two-fold dilutions). **(B-D)** Western blots (WB) analysis of dose-dependent inhibition of ZIKV NS3 expression by temoporfin **(B)**, niclosamide **(C)**, and nitazoxanide **(D)** using the GTX133309 ZIKV α-NS3 antibody (GeneTex) (left panel), respectively. The experiment was performed at the 48 h time point. Middle panel, NS3 expression (lower bands) normalized to the GAPDH loading control. Right panel, accumulated PP normalized to the DMSO control. ***P* < 0.01; ****P* < 0.001. **(E)** MS/MS spectra obtained from the fragmentation of the precursor ion at *m/z* corresponding to representative ZIKV peptides. Fragment ions corresponding to y- and b-ions were observed (red lines).

performed kinetic experiments on the protease (Figure 7A). The V_{max} values for the DENV2 His-NS2B/MBP-NS3 heterocomplex were significantly reduced in the presence of these drugs at various concentrations, compared to the DMSO control. Conversely, the K_m values did not change. The lowered V_{max} but similar K_m values of the His-NS2B/MBP-NS3 heterocomplex indicate non-competitive inhibition according to classical Michaelis-Menten enzyme kinetics. These results are consistent with a proposed mechanism, which posits that these compounds do not compete with the protein substrate at the active site, but instead inhibit protease activity by orthosterically abolishing the binding of NS2B to NS3.

Inhibition of viral polyprotein processing

We asked whether the compounds were also able to inhibit viral protein expression using Western blot analysis. The expression of ZIKV NS3 (~70 KDa) was significantly inhibited by all the drugs in a dose-dependent manner (Figure 7B-7D). For samples treated with temoporfin, niclosamide, and nitazoxanide, an accumulation of high molecular weight (MW) protein (>> 180 KDa) was also observed (Figure 7B-7D), which was absent in the DMSO treated controls. A dose-dependent increase of the high MW protein was seen at temoporfin concentrations ranging from 0.2 to 1.5 μM, and its amount gradually decreased from 3.0 to 6.0 μM. At low concentrations of temoporfin, a clear inverse relationship was observed between the accumulation of the high MW protein and the decrease of NS3 protein expression.

Treatment with low concentrations of niclosamide (0.75 M) and nitazoxanide (3.75 μM) also led to a significant accumulation of high MW protein. At higher drug concentrations (1.5 and 7.5 μM for niclosamide and nitazoxanide, respectively), the accumulation of the high MW protein was less significant and at the very highest drug concentrations, expression of neither NS3 nor the high MW protein level could be detected.

To further characterize the high MW protein, we excised the protein bands, digested them with trypsin, and analyzed them by mass spectrometry. Peptides corresponding to the ZIKV capsid, envelope, NS3, and NS5 proteins were identified (Figure 7E). The mass spectrometry data unambiguously confirmed that the high MW protein was the unprocessed ZIKV PP (~3 391 amino acids).

The unprocessed viral PP accumulates due to inhibition of viral protease by lower concentrations of drugs. For samples treated with drugs at high concentrations, decreased accumulation or absence of PP is likely because of the overall reduced expression of viral protein. Overall, PP accumulation in the presence of drugs indicated that PP processing by the viral protease was inhibited. These results are consistent with our hypothesis that inhibitors preventing NS2B-NS3 interactions abolish protease activity, leading to accumulation of unprocessed PP.

Modeling of binding of drugs to flavivirus NS3 protease

To explore the drugs' potential modes of actions, we docked temoporfin, niclosamide, and nitazoxanide to the crystal structure of the ligand-bound NS3 proteases of DENV3 (PDB ID: 3U1I) [43] and ZIKV (PDB ID: 5LC0) [44] after removing the NS2B peptides. We first employed a SiteMap [45] calculation on NS3pro of DENV3 to identify potential pockets on NS3 for binding of these drugs. The NS3 pockets holding NS2B residues 51 and 53 were ranked as a top site (Supplementary information, Figure S4A and S4B) with the best SiteScore (0.998) and the best Druggability Score (1.050) [46]. The docking results also all supported identification of the 51/53 pockets as the top ranked binding site. We will discuss all our findings based upon docking to these sites.

We then used Autodock Vina [47] to employ an identical docking procedure to dock these drugs to the pockets identified. Overall, the Autodock Vina binding scores for nitazoxanide (−7.2 kcal/mol), niclosamide (−7.5 kcal/mol), and temoporfin (−9.3 kcal/mol) are consistent with the order of their protease inhibition activities (the higher the binding scores, the weaker the potency).

To better explore potential interactions between candidate drugs and NS3, an induced fit docking (IFD)

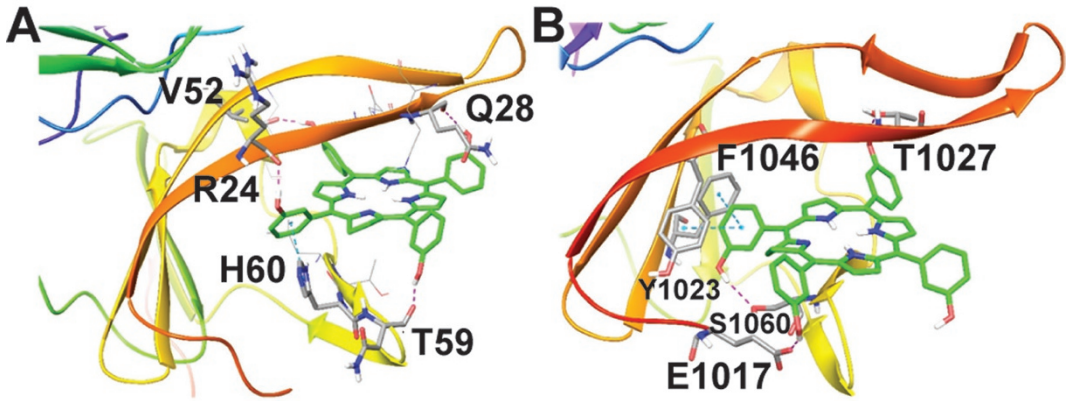

Figure 8 Induced fit docking of drugs to the NS2B 2B51 and 2B53 pockets on NS3pro. **(A**, **B)** Ribbon presentation of temoporfin (green) docked into NS3pro of DENV3 (PDB: 3U1I) **(A)** and ZIKV (PDB: 5LC0) **(B)**, respectively. NS3pro β-strand hairpin loops with residues 25-36 (DENV3) or 1 025-1 036 (ZIKV) are shown in orange and the loops with residues 56-67 (DENV3) or 1 056-1 067 (ZIKV) are shown in yellow. Key interaction residues are highlighted in stick presentation. Hydrogen bonds are shown in purple dotted lines and π-π stacking is shown in blue dotted line.

protocol [45] was employed to accommodate the movements of highly flexible residues upon ligand binding, with 3U1I and 5LC0 as models. All three drugs docked well into the NS3 pockets holding the NS2B residues at positions 51 and 53, termed as 2B51 and 2B53 pockets, respectively (Figure 8A-8B and Supplementary information, Figure S5). Using temoporfin as a model (Figure 8A and 8B), the docking pose shows that temoporfin is tightly sandwiched between two NS3 hairpin loops 25-36 and 56-67. The NS3 residues 24-28 line up along one side of temoporfin, whereas the NS3 residues 58-61 form the other side of the channel. The bottom of the channel is formed by the NS3 residues 23, 25, 53, and 58. Two of the phenol groups of temoporfin are anchored into the 2B51 and 2B53 pockets as shown in the surface presentation of the docking pose (Supplementary information, Figure S4B**)**. The IFD also generated several possible binding poses demonstrating interactions, including hydrogen bonds and π stacking between the ligand and NS3 residues R24, N27, Q28, K33, R54, T59, and H60. These highly flexible NS3 residues are exposed to solvent and likely adopt many different conformations in solution.

The docking result also shows niclosamide and nitazoxanide bind well into the 2B53 pocket in a similar fashion (Supplementary information, Figure S5A-S5D). While their precise binding orientations can be confirmed only by experimental structure determination of the inhibitor-bound NS3 protein, these docked poses of the compounds support the supposition that this hydrophobic pocket in NS3, into which a part of NS2B binds, can reasonably lodge small molecules in the size range of these compounds.

Discussion

The approval of new compounds as drugs by governmental drug administration agencies requires significant effort, time, and expense. If drugs that are already approved for treatment have additional capabilities that can be exploited therapeutically, repurposing them is the fastest route to develop new therapies.

The flavivirus protease enzyme has been considered an encouraging drug target since the outbreak of WNV in the New York City in 1999. As reasoned earlier, the current lack of a successful protease inhibitor drug could be because most of the previous attempts have targeted the flavivirus NS3 protease active site [21-24]. Because the NS2B co-factor binding is essential for the NS3 protease function [13, 14, 48], inhibitors preventing the NS2B-NS3 interaction could provide a promising alternative approach.

In this study, we developed a novel HTS assay to screen the NCGC Pharmaceutical Collection to identify candidate inhibitors blocking interactions between flavivirus NS2B and NS3. Among the three candidate drugs identified, all have encouraging pregnancy profiles with the exception of temoporfin (which has an unknown pregnancy category). Both niclosamide and nitazoxanide fall within the FDA pregnancy category B as substances that fail to demonstrate a risk to the fetus in animal reproduction studies, although there are no adequate and well-controlled studies in pregnant women. In addition, we show for the first time that temoporfin not only has novel anti-flaviviral activities and a novel mechanism of action, but also protects animals from a lethal challenge

by ZIKV.

Temoporfin is a photosensitizer drug approved by the European Union for the treatment of squamous cell carcinoma of the head and neck [30]. Our results show that temoporfin inhibits flavivirus replication via inhibition of the interactions between viral NS2B and NS3 proteins, but not through photoactivation. Currently temoporfin (trade name Foscan) is used as a single dose of 0.15 mg/kg body weight. Temoporfin is a low-clearance substance with a terminal plasma half-life of 65 h in patients [49, 50]. The plasma concentration of temoporfin at 5 days post injection remains above 200 ng/ml (294 nM). Therefore, by a single-dose injection, the blood concentration of temoporfin can be maintained, for at least 5 days, at more than 10-fold EC_{50}, enabling temoporfin to inhibit flaviviruses, including ZIKV. Our data consistently show that temoporfin significantly protects mice from lethal challenge of ZIKV.

Both niclosamide and nitazoxanide are anthelmintic drugs used to treat parasitic infections in human and animals. They are also employed as antivirals against several viruses [51-54]. In addition, an independent qHTS recently identified niclosamide as a potent anti-ZIKV drug, but with unknown mechanism [55]. Our studies indicated that niclosamide is a broad-spectrum flavivirus inhibitor, with similar *in vitro* efficacies for ZIKV, DENV2, WNV, JEV, and YFV. Niclosamide is not considered a developmental toxicant in mammals [56], and is a safe drug even for long-term use. Niclosamide was also reported to effectively treat pregnant women with tapeworm infections [57, 58]. Niclosamide appears to work by killing tapeworms on contact. It is speculated that niclosamide, as an antiviral, acts as a proton carrier to target acidic endosomes, leading to neutralization of cellular endolysosomal pH that will interfere with pH-dependent virus entry [51]. In our studies, niclosamide inhibited virus growth not only at early stage, but more importantly, at 24 h pi (Figure 4H). The results suggest that niclosamide acts at a post-entry step. Our biochemical analyses clearly demonstrate that niclosamide acts as an inhibitor to block the NS2B-NS3 interactions, leading to inactive viral protease and followed by inhibition of viral PP processing. As a consequence of viral PP processing inhibition, viral replication is inhibited. Overall, our data suggest a novel mode of action for niclosamide.

Nitazoxanide is a broad-spectrum antiparasitic drug for the treatment of various helminthic and protozoal infections [59]. Recently, nitazoxanide was found to have broad-spectrum antiviral activity toward viruses, including several members of the Flavividae family [52]. The exact mechanism of action for nitazoxanide's antiviral activity is not well understood. For influenza viruses, nitazoxanide is believed to block maturation of the viral hemagglutinin at the post-translational stage [60]. However, other viruses, including flaviviruses, do not encode hemagglutinin. Our studies demonstrate that nitazoxanide is an effective inhibitor against ZIKV and DENV2, and our results suggest that nitazoxanide inhibits the interactions between the NS3 protease and its co-factor component NS2B. It is possible that nitazoxanide generally serves as a protein-protein interaction (PPI) inhibitor, blocking PPIs necessary for virus replication. Further molecular studies will be required to investigate whether nitazoxanide executes its antiviral activities in other viruses in a way similar to its activity in flaviviruses. Although there are no adequate and well-controlled studies in pregnant woman, research shows nitazoxanide does not adversely affect male or female fertility, nor does it appear to impair fertility or harm the fetus in rats and rabbits [61]. Pharmacokinetic studies indicated that the plasma concentration of nitazoxanide is well above the drug concentration required *in vitro* to inhibit virus growth [62]. Most importantly, *in vivo* studies indicated that nitazoxanide treatment can protect mice from challenge of JEV, a member of flaviviruses [54], suggesting that nitazoxanide may be effective *in vivo* against ZIKV and other flaviviruses as well.

In summary, through a qHTS campaign, we identified and characterized three existing drugs, temoporfin, niclosamide, and nitazoxanide, which can effectively inhibit flaviviruses, including ZIKV. Inhibition occurs through a novel orthosteric mechanism by blocking the interactions of viral proteins NS2B and NS3, which then abolishes the essential viral protease function. Our study also examined infection in primary placenta epithelial cell, stem cell, and neural progenitor populations. The ability for ZIKV to infect human stem cells signifies the immediate threat to a fertilized egg, and infection of neural progenitor cells demonstrates the specificity of ZIKV virus to target an intermediate cell type destined for cortical expansion. Using our antiviral drugs, we established a dose-dependent rescue from viral infection in all ZIKV-relevant cell types. We finally showed that the most potent drug candidate, temoporfin, effectively protects mice from lethal challenge of ZIKV.

Overall, our results demonstrate that flaviviral proteases can be targeted at an orthosteric site, and provide a starting point for further development of orthosteric inhibitors. These findings establish the efficacy of our antiviral drugs to efficiently eliminate infection of ZIKV from human placenta, stem, and progenitor cells, demonstrating a potential means of minimizing the risk of fetal-acquired microcephaly resulting from ZIKV infection of pregnant women [63]. Although further experimenta-

tion will be required to establish whether these drugs can be used prophylactically in treatment of ZIKV-infected patients, including pregnant women, the excellent safety profiles of niclosamide and nitazoxanide suggest such a possibility. It is currently not known whether temoporfin has genotoxicity, nor has it been studied in pregnant women. However, its high anti-flaviviral potency demonstrates its promise as a possible treatment for WNV, JEV, DENV, YFV, and non-pregnant ZIKV patients who may face increased risk of Guillain-Barre syndrome, encephalitis, and other complications. Further studies will be required to evaluate the potential benefits and risks for pregnant patients.

In addition to acute infection, persistent infections have been reported for ZIKV, as well as other flaviviruses [64-66]. Prolonged excretion of ZIKV in sperm and urine has also been reported [67, 68]. It is currently not known how long our studied drugs may be effective pi. Although further investigations may be required, these new findings indicate that the treatment window for ZIKV is relatively large. Nonetheless, the identification of existing drugs as effective inhibitors of ZIKV represents an important first step in managing ZIKV and flaviviruses in general.

Materials and Methods

Compounds

Temoporfin was purchased from Caymen Chemicals, while niclosamide and nitazoxanide were procured from Sigma-Aldrich.

Cloning, expression, and purification

The DENV2 His-NS2B (aa 48-95) was constructed based on an in-house covalently linked N-terminal His-NS2B-NS3 fusion protein, cloned between *Nhe*I and *Eco*R1 sites of the pET28a vector (EMD Biosciences) by introducing a stop codon after Leu95 of the DENV2 NS2B. For cloning of the DENV2 MBP-NS3 protease, an overlapping PCR strategy was used. A DNA fragment of NS3 was amplified with primer pairs MBP-NS3-F and MBP-NS3-R. The PCR product representing the NS3 residues 1-185 was used as a megaprimer for PCR with an in-house His-MBP-Bcl10 constructed in a pDEST-His-MBP vector (Addgene). For His-tagged DENV2 NS3pro, a DNA fragment of NS3 was amplified with primer pairs NS3-F and NS3-R. The PCR product was digested with *Nhe*I and *Bam*HI, and cloned into the pET28a vector (EMD Biosciences). All primers are listed in Supplementary information, Table S1.

The ZIKV NS2B with 3× Flag-tag (DYKDHDGDYKDHDIDYKDDDDKGS) was synthesized by BioBasic and ligated into the pET28a vector (EMD Biosciences) using the *Nde*I and *Eco*RI restriction sites. The ZIKV NS3 was also synthesized by BioBasic and ligated into the pGEX-6P-1 vector (GE HealthCare) using the *Bam*HI and *Eco*RI restriction sites.

Details of the constructs for the HTS assay are as follows: (1) NLuc-NS2B: the N-terminal fragment (aa 1-416) of firefly luciferase (NLuc) was first cloned into the His-NS2B construct between His-tag and NS2B by a megaprimer PCR mutagenesis approach with the primer pair NLUC-NS2B-F and NLUC-NS2B-R; (2) NLuc-E66stop: a stop codon was introduced after the NS2B residue Glu65 by site-directed mutagenesis with primers NLuc-E66stop-F and NLuc-E66stop-R. The construct was named NLuc-E66stop. (3) NS2B-NLuc: the NLuc fragment was placed after NS2B into the His-NS2B-NS3 construct by using the megaprimer PCR mutagenesis approach with primers NS2B-NLuc-F and NS2B-NLuc-R. (4) E66stop-NLuc: the same approach as (3) was used with primers E66stop-NLuc-F and E66stop-NLuc-R. (5) GST-CLuc-NS3 (GCN): the C-terminal fragment (aa 398-550) of firefly luciferase (CLuc398) was amplified using the primer pair Cluc398-F and Cluc398-R, and NS3 was amplified with primer pair GCN-F and GCN-R. CLuc398 and NS3 fusion was amplified using above the PCR products as a template with primers forward CLuc and reverse NS3. The PCR product was then used as a megaprimer for PCR with pGEX-6P-1 vector (GE HealthCare) as a template to generate GST-CLuc398-NS3, named as GCN. (6) GST-NS3-CLuc (GNC): NS3 was amplified using primers GNC-F and GNC-R with an in-house GST-NS3 construct as a template. The PCR product served as a megaprimer PCR mutagenesis approach with an in-house GST-Cluc as template.

All proteins were expressed in *E. coli* strain Rosetta 2(DE3) (EMD Biosciences) and purified through a nickel-nitrilotriacetic acid (NTA) column (Qiagen) or Glutathione sepharose 4B (GE HealthCare), followed by a gel filtration 16/60 Superdex 200 column (GE HealthCare). For refolding of the NS3 protease domain, inclusion bodies were solubilized by 8 M urea in a buffer containing 20 mM Tris, pH 8.0, 500 mM NaCl. Solubilized NS3 was purified through NTA affinity chromatography, and subjected to dialysis with the buffer without urea. The refolded NS3 was centrifuged to clear precipitates and further purified by gel filtration chromatography on a 16/60 Superdex 200 column.

Circular dichroism

CD spectra of the His-MBP-NS3 at 1 mg/ml in PBS buffer were measured on a J-720 Jasco spectropolarimeter (Japan Spectroscopic) equipped with a temperature-controlled cell holder. Static measurements were recorded at 20 ºC. CD spectra were measured at a bandwidth of 1 nm using a quartz cell of path length 0.2 mm for the far-UV (190-260 nm) and a 1-cm quartz cell for the near-UV (250-350 nm). Data from four scans were averaged using the J-720 operating software. Far-UV CD spectra were smoothed using the Jasco noise reduction routine.

Quantitative high-throughput screening assay

The HTS assay was carried out in a 1536-well plate format using a qHTS platform [69]. Compounds were prepared at eight different concentrations (five-fold dilution) in eight different plates. The final concentration of the compounds in the 10-µl assay volume ranged from 0.3 nM to 23 µM. During the primary screen, control inhibitor was used as a positive control and was tested in each plate to evaluate the plate-to-plate consistency. A total of 20 plates were used for 2 816 compounds. In each 32 × 48 (= 1 536) well plate, the first column (32 wells) was a concentration series of control inhibitor in duplicate. The second column was the control inhibitor at the highest concentration, and the third column was DMSO control. Data from the second and third columns were used to estimate data quality indicators such as Z factors and S/B ratios. The Z

factor was defined as $1 - ((3 \times s.d._{DMSO}) + (3 \times s.d._{inhibitor})/ (Mean_{DMSO} - Mean_{inhibitor}))$, and S/N was defined as $Mean_{DMSO}/Mean_{inhibitor}$. The GCN protein (80 nM final concentration) was dispensed into test buffer (1× phosphate buffered saline (PBS), 0.05% Chaps, 0.1% BSA, 0.5% DMSO) with compounds from the NCGC Pharmaceutical Collection at various concentrations, and incubated for 30 min. Then the NLuc-E66stop was added to the mixture to a final concentration of 80 nM. The D-luciferin substrate (Gold Biotechnology) dissolved in substrate buffer composing of 1× PBS, 2 mM $MgCl_2$, 4 mM EGTA, 4 mM ATP, 1 mM DTT was added to a final concentration of 5 μg/ml. The reaction mixture was incubated to 2 h at room temperature and read using a ViewLux Plate Reader.

Data were processed as reported previously [69]. Briefly, raw plate reads for each titration point were first normalized relative to control inhibitor (100 %) and DMSO-only wells (basal, 0%), and then corrected by applying a pattern correction algorithm using compound-free control plates (DMSO plates). Concentration-response titration points for each compound were fitted to the Hill equation, yielding EC_{50} and maximal response (efficacy) values. Compounds from qHTS were classified into four major classes (curve class 1-4) based on quality of curve fit and efficacy using criteria published in ref. [69]. We have the highest confidence in class 1.1 (efficacy > 80% with both upper and lower asymptotes), 1.2 (efficacy 30%-80% with both upper and lower asymptotes), or 2.1 (efficacy > 80% with one asymptote) concentration curves, and have less confidence in class 2.2 (efficacy < 80% with one asymptote) and 3 (single point activity) curves. Class 4 compounds that showed no concentration response indicated inactive compounds. Active compounds with curve classes 1.1, 1.2, or 2.1 were selected for confirmation experiment.

In a cherry-picking confirmation experiment, selected active compounds were re-tested in 11 point titrations with concentrations ranging from 390 pM to 23 μM (three-fold dilution) in the SLC assay. These tests used the same protocol as described above, except that 11 point titrations were within one 1 536-well plate.

Protease inhibition assay

The DENV2 NS3-MBP fusion protein (50 nM) was mixed with candidate compounds (at various concentrations or DMSO control) in reaction buffer (20 mM Tris pH 8.0, 100 mM NaCl, 5% Glycerol, and 0.05% CHAPS) and incubated at 4 °C for 30 min. The DENV2 His-NS2B was then added at 1 μM final concentration. The peptide substrates (Abz-RRRRSAG-nTyr (NeoBiolab) or TAMRA-RRRRSAG-GXL570 (AnaSpec) were added to the mixture at a concentration of 50 or 10 μM, respectively, and substrate cleavage was monitored over time at 37 °C in a BioTek Flx800 at excitation/emission wavelengths of 360/420 nm (Abz substrate) or 520/575 nm (TAMRA substrate). The rate of increase in RFU over time was calculated in the linear range and normalized as Δfluorescence defined as $RFU_{final} - RFU_0$.

For all bar graphs and dose-responsive curves, all data were presented as means and s.d. of experimental data in triplicate, or as specified. Sigmoidal function within the Origin Suite 6.0 (Origin Lab, Wellesley Hills, MA, USA) was used for dose-responsive curve fittings, unless otherwise specified.

Cytotoxicity assay

Cytotoxicity for temoporfin was measured by a MTT cell proliferation assay using the 3-(4,5-dimethylthiazol-2-yl)-2,5-diphenyl tetrazolium bromide method (ATCC), as described previously [70, 71]. Because niclosamide and nitazoxanide have spectra absorption interfering with the MTT assay, cytotoxicity for these compounds was measured by a WST-8 cell proliferation assay (Dojindo Molecular Technologies), according to manufacturer's protocol. Briefly, ~1×10^5 cells in 100 μl of media were seeded into 60 wells of a 96-well plate, while the remaining wells held media. Plates were held at RT for 1 h and then incubated for 20-24 h. The media was removed, and 100 μl of media containing decreasing concentrations of antiviral compound in 1% DMSO were added to the wells. All determinations were performed in triplicate. After 42 h incubation at 37 °C, MTT or WST-8 assays were performed according to manufacturers' protocols. A microtiter plate reader (Ely808, BioTek Instruments) with a 570 nm filter (MTT) or 450 nM (WST-8) was used to record absorbance. After adjusting the absorbance for background and comparing to untreated controls, the cytotoxic concentration CC_{50} was calculated using a sigmoidal nonlinear regression function to fit the dose-response curve using the ORIGIN Suite 6.0 (Origin Lab).

Viral titer reduction assays

A viral titer reduction assay was used to determine the compound's effect on selected flaviviruses, including DENV2, ZIKV (Puerto Rico strain PRVABC59), WNV, JEV, and YFV, using A549 cells (American Type Culture Collection) as described previously [70, 71]. Briefly, ~2×10^5 human A549 cells in 500 μl of media were seeded into each well of a 24-well plate. At 24 h after seeding, dilutions at 2× the desired concentration of the compound were made in 1% DMSO media and 250 μl was added to wells in triplicate. Immediately following, 250 μl of media containing viruses at a concentration to yield a MOI 0.1 PFU/cell was added to the wells. After 42 h incubation at 37 °C, culture media were collected and stored at −80 °C for later quantification using a plaque assay. For the plaque assay, Vero cell monolayers in six-well plates were seeded 3-4 days prior to infection to achieve a confluent monolayer. Depending on the virus, 3-8 10-fold serially dilutions of the harvested samples were made. To inoculate, 100 μl of the dilution is inoculated into each of two wells, rocked gently to distribute virus, and incubated for 1 h at 37 °C. Cells are then overlaid with a nutrient medium containing 0.6% oxoid agar. The agar is allowed to solidify and the plates are then incubated at 37 °C. A second overlay containing 2% neutral red is added after the plaques begin to appear on day 2, and then incubated overnight. Plaques are counted daily for 1-3 days until no significant increase is seen. The effective concentration EC_{50} was determined by sigmoidal nonlinear regression fitting of the dose-response curve using the ORIGIN software package.

HPECs derived from the inner surface of the amnion were purchased from Cell Applications, and cultured according to manufacturer's manual. Human hNPC, derived from iPSC generated using the STEMCCA Cre-Excisable Constitutive Polycistronic (OKSM) lentivirus, was purchased from EMD Millipore, and cultured according to manufacturer's manual.

The human iPS cell line IPSC-HDF9 [37] was cultured and maintained on pre-coated matrigel (BD Biosciences) plates and fed every 24 h using mTSeR medium (Stemcell Technologies). Cell lines were passaged at a 1:6 ratio after 70-80% confluency using Dispase (Stemcell Technologies) and a cell scraper for gentle dissociation. Cells were manually picked, washed with DMEM,

and re-plated onto matrigel-coated plates when necessary to ensure high-quality undifferentiated colonies. Undifferentiated iPSCs were counted with a hemocytometer and replated on matrigel at 200 000 cells per 24-well plate or 20 000 cells per 96-well plate before infection with ZIKV.

The antiviral efficacy experiments with HPECs, hNPCs, and iPSC HDF9 were carried out as described [70, 71], except that HPECs, hNPCs, or iPSC HDF9 were used instead of A549 cells and a MOI of 2.

The *in vitro* antiviral activity of temoporfin to a contemporary ZIKV strain GZ01 [72] (isolated from patient returned from Venezuela in 2016) was carried out as previously described [73]. Briefly, Vero cells were infected with Zika virus GZ01/2016 strain at a MOI of 0.1 and treated with 10-fold serial dilutions of temoporfin. About 0.5% DMSO was added to virus-infected cells as a negative control. At day 2 pi, viral RNAs were extracted from infected cells with PureLink RNA Mini Kit (Life Technologies, USA) according to the manufacturer's recommendation and detected by qRT-PCR assays with the One-Step PrimeScript RT-PCR Kit (Takara, Japan) using the ZIKV-specific primers.

All cells were tested as free of Mycoplasma contamination.

Immunofluorescence assay

ZIKV-infected cells treated with DMSO or drugs were grown in 96-well black imaging plates (Corning). At 48-h pi, growth medium was removed. The cells were washed once with PBS and fixed on ice in 100% pre-chilled (−20 °C) methanol for 15 min. The fixed cells were incubated for 1 h with blocking and permeabilisation buffer containing 0.5% Triton X-100, 0.2 μg/ml EDTA, and 1% BSA in PBS. The cells were then treated with a mouse monoclonal pan anti-E antibody 4G2 (ATCC) overnight and washed three times with PBST buffer (1× PBS with 0.2% Tween 20). The cells were then incubated with the DyLight 488 goat anti-mouse IgG (ImmunoReagents) for 1 h in blocking buffer, after which the cells were washed three times with PBST. Nuclear staining dye Hoechst was added and incubated for 5 min. Fluorescence images were recorded under a fluorescence microscope equipped with an Olympus DP71 imaging system.

Quantitative qRT-PCR

About 50 μl of cell supernatant samples was extracted on Applied Biosystems MagMAX Express-96 Deep Well Magnetic Particle Processor. TaqMan gene expression qRT-PCR assays were performed with 5μl of the extracted RNA using the TaqMan One-step RT-PCR Master Mix Reagents Kit (PE Biosystems) on Applied Biosystems 7500 Real-time PCR System. TaqMan primers for ZIKV are 5'-CCGCTGCCCAACACAAG-3' and 5'-CCACTAAYGTTCTTTTGCAGACAT-3' with ZIKV probe Cy5 5'-AGCCTACCT/TAO/TGACAAGCAGTCAGACACTCAA-3' IAbRQSp. Samples were analyzed by relative quantification using the 2−ΔΔCT ("delta-delta Ct") compared with the endogenous control.

Protein thermal shift assay

The PTSA was conducted using an Applied Biosystem 7500 Fast Real-Time PCR System (ThermoFisher Scientific) from 25 to 80 °C. The DENV2 His-MBP-NS3 (final concentration of 2.5 μM in 1× PBS) was mixed with each compound to attain a 4.8 μM final concentration in 1.6% DMSO in the MicroAmp Fast Optical 96-Well Reaction Plate (ThermoFisher Scientific). Thermal denaturation was monitored using SYPRO Orange (Life Technologies) according to manufacturer's manual. The denaturation of the proteins was monitored by following the increase of the fluorescence emitted by the probe that binds exposed hydrophobic regions of the denatured protein. The melting temperature (T_m) was calculated as the mid-log of the transition phase from the native to the denatured protein, using a derivative model using the Protein Thermal Shift Software v1.0 (ThermoFisher Scientific). The reference unfolding temperature of proteins in 1.6% DMSO (T_{m-DMSO}) was subtracted from the values in the presence of each compounds (T_{m-comp}) to obtain thermal shifts, $\Delta T_m = T_{m-comp} - T_{m-DMSO}$. Compounds were considered to be binders when $\Delta T_m > 0.5$ °C.

Competitive GST pull-down assay

GST or GST-NS3 (100 μg) were immobilized on glutathione-sepharose 4B beads (GE HealthCare) and aliquoted at 10 μg/tube. Drugs at two-fold dilutions were applied to the aliquoted beads, and incubated at 4 °C overnight. Then FLAG-tagged NS2B (10 μg) was applied to each reaction and incubated at 4 °C for 2 h. The incubated beads were washed four times with a PBSC buffer containing PBS with 0.05% CHAPS, and subjected to western blot analysis using anti-FLAG antibody (A00170-40, Genscript) or anti-GST antibody (27-4577-01, GE HealthCare). All experiments were triplicated.

Surface plasmon resonance

Affinity and kinetic analyses of the interactions between each drug and the His-NS3 protease domain were determined using a ProteOn XPR36 SPR instrument (Bio-Rad) at 25 °C. Refolded His-NS3 was immobilized (~15 000 RU) onto a ProteOn GLH sensor chip (Bio-Rad). The concentrations used for the injected compounds ranged from 1 μM to 37 nM (temoporfin), from 9 μM to 333 nM (niclosamide), and from 10 μM to 370 nM (nitazoxanide), with three-fold dilutions. A blank surface blocked by ethanolamine was used as the control surface. To minimize nonspecific binding, we carried out all the binding experiments in a PBSTD buffer containing 1× PB, 0.005% surfactant P20, and 5% DMSO, at a flow rate of 100 μl/min. Association (k_a) and dissociation (k_d) rates, as well as the dissociation constant (K_D), were obtained by global fitting of the SPR data from multiple concentrations to a simple 1:1 Langmuir binding model, using the ProteOn Manager software suite (Bio-Rad).

Western blot

ZIKV-infected A549 cells treated with DMSO or drugs were washed twice with PBS buffer and manually scraped out of the six-well plates. Cells were spun down and supernatant was removed. About 30 μl of complete protease inhibitor cocktail in PBS was added to the cells, followed by addition of 30 μl of SDS-PAGE loading buffer. The mixtures were boiled at 95 ºC for 10 min, followed by centrifugation at 15 000 rpm for 10 min. Sample was analyzed using 12% SDS-PAGE. The primary antibodies used were anti-ZIKV NS3 (GTX133309, GeneTex) and anti-GAPDH (CB1001, EMD Millipore).

Mass spectrometry

The protein band of interest on SDS-PAGE gel was manually excised. The pieces were dehydrated with acetonitrile for 10 min,

vacuum dried, rehydrated with 5 mM triphosphine hydrochloride in 50 mM ammonium bicarbonate (pH 8.5) at 37 °C for 1 h, and then alkylated with 100 mM iodoacetamide in 50 mM ammonium bicarbonate (pH 8.5) at room temperature for 1 h. The pieces were washed twice with 50% acetonitrile, dehydrated with acetonitrile for 10 min, dried, and digested with a total of 25 ng of sequencing grade modified trypsin (Sigma-Aldrich) in 50 mM ammonium bicarbonate (pH 8.5) at 37 °C overnight. Following digestion, tryptic peptides were extracted three times with 50% acetonitrile containing 5% formic acid for 15 min each time while being vortexed. The extracted solutions were pooled and evaporated under vacuum prior to MS analysis.

The peptides were re-suspended in 60 µl of 0.1% vol/vol formic acid and separated on a CapLC system (Waters, Milford, MA, USA) coupled to a QSTAR XL (ABSCIEX, Framingham, MA, USA). Peptides were desalted onto an Everest C18 (5 µm, 500 µm ID × 15 mm, Grace, Deerfield, IL, USA) with solvent A (97:3 H_2O:ACN with 0.1% vol/vol formic acid and 0.01% vol/vol TFA) at 40 µl/min. After a 6-min wash, peptides were separated on a Jupiter C18 (3 µm, 100 µm ID × 150 mm, Phenomenex, Torrance, CA, USA) using a 40-min linear gradient of 10%-40% solvent B (85% ACN/10% isopropanol + 0.1% vol/vol formic acid + 0.0075% vol/vol TFA) at 250 nl/min. MS data acquisition was performed using Analyst QS 1.1 software (ABSciex) in positive ion mode for information-dependent acquisition (IDA) analysis. The nanospray voltage was 2.1 kV used for all experiments in a positive ion mode. Nitrogen was used as the curtain (value of 20) with heated interface at 130 °C. The declustering potential was set at 80 eV and Gas1 was 5 (arbitrary unit). In IDA analysis, after each survey scan from *m/z* 350 to 1 200, the three highest intensity ions above the predefined threshold 28 cps with multiple charge states (+ 2 and + 3) were selected for tandem MS (MS/MS), with rolling collision energy applied for detected ions based on different charge states and *m/z* values. Each MS/MS acquisition was completed and switched back to survey scan when the precursor intensity fell below a predefined threshold or after a maximum of 65 s acquisition. After data acquisition, the individual MS/MS spectra acquired for each precursor within a single LC run were combined, smoothed, deisotoped using an Analyst "script" mascot.dll to create a peak list, and the peak list was saved to a file. Then the peak list file was used to query viral protein and contaminant data subsets using the MASCOT 2.5 from Matrix Science (London, UK) with the following parameters: peptide mass tolerance, 0.3 Da; MS/MS ion mass tolerance, 0.3 Da; allow up to two missed cleavage. Several variable modifications were applied, including methionine oxidation and cysteine carbamidomethylation. Only significant scores for the peptides defined by Mascot probability analysis (http://www.matrixscience.com/help/scoring_help.html#PBM) greater than "identity" with 95% confidence were considered for the peptide identification.

Modeling

The NS2B-bound crystal structures of the DENV3 (PDB ID: 3U1I) were downloaded from RCSB PDB Bank. To prepare the NS3 protease structure for the mapping task, ligands and cofactors were removed, hydrogens were added, and crystal waters were removed. The SiteMap Calculation was run from the Schrödinger Maestro [45] SiteMap panel. The task of identifying top-ranked potential receptor binding site was specified and a fine grid spacing of 0.7 Å was selected. The OPLS_2005 force field was used for calculation. The result from the mapping was then incorporated into Maestro for visualization and evaluation.

The 3D structures for niclosamide, nitazoxanide, and temoporfin were downloaded in SDF format from the ZINC15 library [74]. The NS2B-bound crystal structures of the Dengue NS3 protease (PDB ID: 3U1I [43]) and of the Zika NS3 protease (PDB ID: 5LC0 [44]) were used as docking targets to predict the possible bound conformations of these compounds. The program Autodock Vina [47] was used to dock the molecules into two putative binding sites corresponding to two NS2B residues that bind to NS3: L51/M51 and V53/I53. The Cartesian coordinates of the CB atom of each of these residues were used as the center of the box used for docking in the respective structure. Ligand boxes extended 25 Å in each direction, and an exhaustiveness parameter of 16 was used for the docking.

In order to generate more accurate ligand poses and accommodate the movements of highly flexible residues on NS3 protease, an IFD protocol of Schrödinger Small-Molecule Drug Discovery Suite [45] was employed in this docking study. Crystal structures of DENV3 (PDB Code: 3U1I) and ZIKV (PDB Code: 5LC0) were used as docking templates. Only the NS3 protease was kept from each structure and prepared with Protein Prepared Wizard. During this step, hydrogens were added, crystal waters were removed, partial charges were assigned using the OPLS-2005 force field, and protonation states were assigned. The 3D conformations of ligands were created using the Schrödinger Maestro and prepared with LigPrep. During this step, a single, low energy, 3D structure of each ligand was produced. The IFD protocol was run from Schrödinger Maestro using the IFD panel. On NS3 chains of DENV3 and ZIKV, the center of box for docking was chosen on the centroid of a set of selected residues within the 2B53 pocket. The box size was set to 26 Å on each side. Selected side chains (R24, K26, and T59 of DENV3; M1026, S1060, and Y1023 of ZIKV) were temporarily removed (equivalent of being temporarily mutated to alanine) to create more space during the initial IFD process and were restored after the docking step. The IFD procedure used reduced van der Waals radii scaling (0.7 for nonpolar receptor atoms and 0.5 for nonpolar ligand atoms) for a flexible docking. For each pose generated from initial Glide docking, a Prime structure prediction was then used to accommodate the ligand by reorienting nearby side chains. These residues and the ligand were then minimized. During this process, the receptor structures were optimized. Finally, each ligand was re-docked into the structures within 30 kcal/mol, and within the top 20 structures using Glide XP mode. As a result, multiple docking poses were generated and ranked according to the IFD scores. The poses with lower values of IFD scores are more favorable for binding. The receptor-ligand complexes structures were imported into Schrödinger Maestro for visualization and analysis of binding site interactions.

In vivo protection efficacy

All animal studies involving infectious ZIKV were conducted at an animal biosafety level 2 (ABSL-2) facility at Beijing Institute of Microbiology and Epidemiology with Institutional Biosafety Committee approval (IACUC-13-2016-001). The *in vivo* antiviral activity of temoporfin was evaluated in two established animal models.

For the viremia model in immunocompetent Balb/C mice [39,

40], a group of 3-week-old female Balb/c mice infected intraperitoneally (ip) with 2×10^5 PFU of ZIKV strain GZ01/2016 were ip administered temoporfin at 0.02 mg/mice (n = 8) or vehicle control (n = 7) every day for 2 consecutive days post infection (dpi). Viremia on day 2 pi was determined by RT-qPCR, and statistical analysis was performed using the unpaired, two-tailed t-test.

For the lethal A129 mice model [41, 42], a group of 4-week old A129 mice were infected ip with 2×10^5 PFU of ZIKV GZ01/2016 strain. Then, the infected mice were ip administered with temoporfin at 1 mg/kg of body weight (n = 12) or with vehicle control (n = 10) every day for 5 consecutive dpi. Mice were observed daily for signs of illness and mortality. Survival curves were compared using the Log-rank test.

Statistical analysis

All experiments were performed in triplicates unless specified otherwise. Western blots were quantified using the Bio-Rad Gel Doc EZ system and Image Lab software #1709690 (Bio-Rad). One-way ANOVA was used to carry out statistical analyses with the Prism software, unless otherwise specified. Survival curves were compared using the Log-rank test.

Acknowledgments

We thank J Tang at the Wadsworth Center Tissue Culture Core facility for help in cell culture, E Eisele at the Biochemistry Core for assistance in CD experiments, and other core facilities at the Wadsworth Center, including the Applied Genomic Technologies Core for DNA sequencing, the Advanced Light Microscopy Core for immunofluorescence imaging, and the Tissue Culture Core for media. We also thank X Zhao at the University of Wisconsin-Madison for helpful discussion of neural progenitor cells. MB was partially supported by the NIH Biodefense and Emerging Infectious Disease training grant AI055429. CFQ was supported by the National Natural Science Foundation of China (NSFC) Excellent Young Scientist (81522025), Innovative Research Group (81621005), the National Key Research and Development Project of China (2016YFD0500304), the National Science and Technology Major Project of China (2017ZX09101005), and the Newton Advanced Fellowship from the UK Academy of Medical Sciences (NAF003\1003) and the NSFC (81661130162). BL was partially supported by a visiting scholarship sponsored by Guangdong Ocean University. FG was partially supported by a visiting scholarship sponsored by the China Scholarship Council. This work was partially supported by the Wadsworth Center flavivirus drug discovery seed funding (HL, NB, and LDK), by NIH grant DA038446 (JZ), and by the Intramural Research Program of NCATS, NIH (MX).

Author Contributions

ZL, MB, YQD, JZ, SS, BL, RH, CAK, CAA, SAJ, HC, NNZ, MT, FG, and QL performed experiments; ZL, MB, QL, NB, JZ, NB, MX, LDK, CFQ, and HL designed the study, interpreted data, and wrote the manuscript.

Competing Financial Interests

The authors declare no competing financial interests.

References

1 Calvet G, Aguiar RS, Melo AS, *et al.* Detection and sequencing of Zika virus from amniotic fluid of fetuses with microcephaly in Brazil: a case study. *Lancet Infect Dis* 2016; **16**:653-660.
2 Chen LH, Hamer DH. Zika Virus: rapid spread in the western hemisphere. *Ann Intern Med* 2016; **164**:613-615.
3 Govero J, Esakky P, Scheaffer SM, *et al.* Zika virus infection damages the testes in mice. *Nature* 2016; **540**:438-442.
4 Ma W, Li S, Ma S, *et al.* Zika virus causes testis damage and leads to male infertility in mice. *Cell* 2016; **167**:1511-1524. e15.
5 Miner JJ, Sene A, Richner JM, *et al.* Zika virus infection in mice causes panuveitis with shedding of virus in tears. *Cell Rep* 2016; **16**:3208-3218.
6 Yepez JB, Murati FA, Pettito M, *et al.* Ophthalmic manifestations of congenital Zika syndrome in Colombia and Venezuela. *JAMA Ophthalmol* 2017; **135**:440-445.
7 Thomas DL, Sharp TM, Torres J, *et al.* Local transmission of Zika virus - Puerto Rico, November 23, 2015-January 28, 2016. *MMWR Morb Mortal Wkly Rep* 2016; **65**:154-158.
8 Martines RB, Bhatnagar J, Keating MK, *et al.* Notes from the field: evidence of Zika virus infection in brain and placental tissues from two congenitally infected newborns and two fetal losses - Brazil, 2015. *MMWR Morb Mortal Wkly Rep* 2016; **65**:159-160.
9 Rodriguez-Morales AJ. Zika and microcephaly in Latin America: an emerging threat for pregnant travelers? *Travel Med Infect Dis* 2016; **14**:5-6.
10 Baud D, Van Mieghem T, Musso D, Truttmann AC, Panchaud A, Vouga M. Clinical management of pregnant women exposed to Zika virus. *Lancet Infect Dis* 2016; **16**:523.
11 Mecharles S, Herrmann C, Poullain P, *et al.* Acute myelitis due to Zika virus infection. *Lancet* 2016; **387**:1481.
12 Carteaux G, Maquart M, Bedet A, *et al.* Zika virus associated with meningoencephalitis. *N Engl J Med* 2016; **374**:1595-1596.
13 Chambers TJ, Grakoui A, Rice CM. Processing of the yellow fever virus nonstructural polyprotein: a catalytically active NS3 proteinase domain and NS2B are required for cleavages at dibasic sites. *J Virol* 1991; **65**:6042-6050.
14 Falgout B, Pethel M, Zhang YM, Lai CJ. Both nonstructural proteins NS2B and NS3 are required for the proteolytic processing of dengue virus nonstructural proteins. *J Virol* 1991; **65**:2467-2475.
15 Chappell KJ, Stoermer MJ, Fairlie DP, Young PR. Mutagenesis of the west Nile virus NS2B cofactor domain reveals two regions essential for protease activity. *J Gen Virol* 2008; **89**:1010-1014.
16 Niyomrattanakit P, Winoyanuwattikun P, Chanprapaph S, Angsuthanasombat C, Panyim S, Katzenmeier G. Identification of residues in the dengue virus type 2 NS2B cofactor that are critical for NS3 protease activation. *J Virol* 2004; **78**:13708-13716.
17 Zhang Z, Li Y, Loh YR, *et al.* Crystal structure of unlinked NS2B-NS3 protease from Zika virus. *Science* 2016; **354**:1597-1600.
18 Phoo WW, Li Y, Zhang Z, *et al.* Structure of the NS2B-NS3

protease from Zika virus after self-cleavage. *Nat Commun* 2016; **7**:13410.
19 Lei J, Hansen G, Nitsche C, Klein CD, Zhang L, Hilgenfeld R. Crystal structure of Zika virus NS2B-NS3 protease in complex with a boronate inhibitor. *Science* 2016; **353**:503-505.
20 Chen X, Yang K, Wu C, *et al.* Mechanisms of activation and inhibition of Zika virus NS2B-NS3 protease. *Cell Res* 2016; **26**:1260-1263.
21 Luo D, Vasudevan SG, Lescar J. The flavivirus NS2B-NS3 protease-helicase as a target for antiviral drug development. *Antiviral Res* 2015; **118**:148-158.
22 Lim SP, Wang QY, Noble CG, *et al.* Ten years of dengue drug discovery: progress and prospects. *Antiviral Res* 2013; **100**:500-519.
23 Sampath A, Padmanabhan R. Molecular targets for flavivirus drug discovery. *Antiviral Res* 2009; **81**:6-15.
24 Brecher M, Zhang J, Li H. The flavivirus protease as a target for drug discovery. *Virol Sin* 2013; **28**:326-336.
25 Pambudi S, Kawashita N, Phanthanawiboon S, *et al.* A small compound targeting the interaction between nonstructural proteins 2B and 3 inhibits dengue virus replication. *Biochem Biophys Res Commun* 2013; **440**:393-398.
26 Bi K, Nishihara K, Machleidt T, *et al.* Identification of known drugs targeting the endoplasmic reticulum stress response. *Anal Bioanal Chem* 2015; **407**:5343-5351.
27 Baell JB, Holloway GA. New substructure filters for removal of pan assay interference compounds (PAINS) from screening libraries and for their exclusion in bioassays. *J Med Chem* 2010; **53**:2719-2740.
28 Wu CF, Wang SH, Sun CM, Hu ST, Syu WJ. Activation of dengue protease autocleavage at the NS2B-NS3 junction by recombinant NS3 and GST-NS2B fusion proteins. *J Virol Methods* 2003; **114**:45-54.
29 Phong WY, Moreland NJ, Lim SP, Wen D, Paradkar PN, Vasudevan SG. Dengue protease activity: the structural integrity and interaction of NS2B with NS3 protease and its potential as a drug target. *Biosci Rep* 2011; **31**:399-409.
30 Lorenz KJ, Maier H. Squamous cell carcinoma of the head and neck. Photodynamic therapy with Foscan. *HNO* 2008; **56**:402-409.
31 O'Connor AE, Gallagher WM, Byrne AT. Porphyrin and nonporphyrin photosensitizers in oncology: preclinical and clinical advances in photodynamic therapy. *Photochem Photobiol* 2009; **85**:1053-1074.
32 Tabata T, Petitt M, Puerta-Guardo H, *et al.* Zika virus targets different primary human placental cells, suggesting two routes for vertical transmission. *Cell Host Microbe* 2016; **20**:155-166.
33 Tang H, Hammack C, Ogden SC, *et al.* Zika virus infects human cortical neural progenitors and attenuates their growth. *Cell Stem Cell* 2016; **18**:587-590.
34 Zhang F, Hammack C, Ogden SC, *et al.* Molecular signatures associated with ZIKV exposure in human cortical neural progenitors. *Nucleic Acids Res* 2016.
35 Qian X, Nguyen HN, Song MM, *et al.* Brain-region-specific organoids using mini-bioreactors for modeling ZIKV exposure. *Cell* 2016; **165**:1238-1254.
36 Garcez PP, Loiola EC, Madeiro da Costa R, *et al.* Zika virus impairs growth in human neurospheres and brain organoids. *Science* 2016; **352**:816-818.
37 Green MD, Chen A, Nostro MC, *et al.* Generation of anterior foregut endoderm from human embryonic and induced pluripotent stem cells. *Nat Biotechnol* 2011; **29**:267-272.
38 Chambers SM, Fasano CA, Papapetrou EP, Tomishima M, Sadelain M, Studer L. Highly efficient neural conversion of human ES and iPS cells by dual inhibition of SMAD signaling. *Nat Biotechnol* 2009; **27**:275-280.
39 Zhang NN, Tian M, Deng YQ, *et al.* Characterization of the contemporary Zika virus in immunocompetent mice. *Hum Vaccin Immunother* 2016; **12**:3107-3109.
40 Larocca RA, Abbink P, Peron JP, *et al.* Vaccine protection against Zika virus from Brazil. *Nature* 2016; **536**:474-478.
41 Dai L, Song J, Lu X, *et al.* Structures of the Zika virus envelope protein and its complex with a flavivirus broadly protective antibody. *Cell Host Microbe* 2016; **19**:696-704.
42 Lazear HM, Govero J, Smith AM, *et al.* A mouse model of Zika virus pathogenesis. *Cell Host Microbe* 2016; **19**:720-730.
43 Noble CG, Seh CC, Chao AT, Shi PY. Ligand-bound structures of the dengue virus protease reveal the active conformation. *J Virol* 2012; **86**:438-446.
44 Lei J, Hansen G, Nitsche C, Klein CD, Zhang L, Hilgenfeld R. Crystal structure of Zika virus NS2B-NS3 protease in complex with a boronate inhibitor. *Science* 2016; **353**:503-505.
45 Small-Molecule Drug Discovery Suite 2016-3: Schrödinger Suite 2016-3, Schrödinger, LLC, New York, NY, 2016.
46 Nayal M, Honig B. On the nature of cavities on protein surfaces: application to the identification of drug-binding sites. *Proteins* 2006; **63**:892-906.
47 Trott O, Olson AJ. AutoDock Vina: improving the speed and accuracy of docking with a new scoring function, efficient optimization, and multithreading. *J Comput Chem* 2010; **31**:455-461.
48 Chambers TJ, Hahn CS, Galler R, Rice CM. Flavivirus genome organization, expression, and replication. *Annu Rev Microbiol* 1990; **44**:649-688.
49 Triesscheijn M, Ruevekamp M, Out R, *et al.* The pharmacokinetic behavior of the photosensitizer meso-tetra-hydroxyphenyl-chlorin in mice and men. *Cancer Chemother Pharmacol* 2007; **60**:113-122.
50 Glanzmann T, Hadjur C, Zellweger M, *et al.* Pharmacokinetics of tetra(m-hydroxyphenyl)chlorin in human plasma and individualized light dosimetry in photodynamic therapy. *Photochem Photobiol* 1998; **67**:596-602.
51 Jurgeit A, McDowell R, Moese S, Meldrum E, Schwendener R, Greber UF. Niclosamide is a proton carrier and targets acidic endosomes with broad antiviral effects. *PLoS Pathog* 2012; **8**:e1002976.
52 Rossignol JF. Nitazoxanide: a first-in-class broad-spectrum antiviral agent. *Antiviral Res* 2014; **110**:94-103.
53 Fang J, Sun L, Peng G, *et al.* Identification of three antiviral inhibitors against Japanese encephalitis virus from library of pharmacologically active compounds 1280. *PLoS One* 2013; **8**:e78425.
54 Shi Z, Wei J, Deng X, *et al.* Nitazoxanide inhibits the replication of Japanese encephalitis virus in cultured cells and in a mouse model. *Virol J* 2014; **11**:10.
55 Xu M, Lee EM, Wen Z, *et al.* Identification of small-mole-

cule inhibitors of Zika virus infection and induced neural cell death via a drug repurposing screen. *Nat Med* 2016; **22**:1101-1107.
56 Krieger R. ed. Inhibitors and Uncouplers and Antiparasitic Agents. San Diego, CA: Academic Press, 2001.
57 Galan-Puchades MT, Fuentes MV, Mas-Coma S. Human Bertiella studeri in Spain, probably of African origin. *Am J Trop Med Hyg* 1997; **56**:610-612.
58 Asnis D, Kazakov J, Toronjadze T, *et al.* Neurocysticercosis in the infant of a pregnant mother with a tapeworm. *Am J Trop Med Hyg* 2009; **81**:449-451.
59 White CA Jr. Nitazoxanide: a new broad spectrum antiparasitic agent. *Expert Rev Anti Infect Ther* 2004; **2**:43-49.
60 Rossignol JF, La Frazia S, Chiappa L, Ciucci A, Santoro MG. Thiazolides, a new class of anti-influenza molecules targeting viral hemagglutinin at the post-translational level. *J Biol Chem* 2009; **284**:29798-29808.
61 ROMARK. Available from:.http://www.accessdata.fda.gov/drugsatfda_docs/label/2005/021818lbl.pdf
62 Balderas-Acata JI, Ríos-Rogríguez Bueno EP, Pérez-Becerril F, Espinosa-Martínez C, Burke-Fraga V, la Parra MG. Bioavailability of two oral-suspension formulations of a single dose of nitazoxanide 500 mg: an open-label, randomized-sequence, two-period crossover, comparison in healthy fasted mexican adult volunteers. *J Bioequiv Availab* 2011; **3**:43-47.
63 Lessler J, Chaisson LH, Kucirka LM, *et al.* Assessing the global threat from Zika virus. *Science* 2016; **353**:aaf8160.
64 Robbiani DF, Bozzacco L, Keeffe JR, *et al.* Recurrent potent human neutralizing antibodies to Zika virus in Brazil and Mexico. *Cell* 2017; **169**:597-609.e11.
65 Murray KO, Gorchakov R, Carlson AR, *et al.* Prolonged detection of Zika virus in vaginal secretions and whole blood. *Emerg Infect Dis* 2017; **23**:99-101.
66 Suy A, Sulleiro E, Rodo C, *et al.* Prolonged Zika virus viremia during pregnancy. *N Engl J Med* 2016; **375**:2611-2613.
67 Hirsch AJ, Smith JL, Haese NN, *et al.* Zika virus infection of rhesus macaques leads to viral persistence in multiple tissues. *PLoS Pathog* 2017; **13**:e1006219.
68 Barzon L, Pacenti M, Franchin E, *et al.* Infection dynamics in a traveller with persistent shedding of Zika virus RNA in semen for six months after returning from Haiti to Italy, January 2016. *Euro Surveill* 2016; **21**:30316.
69 Inglese J, Auld DS, Jadhav A, *et al.* Quantitative high-throughput screening: a titration-based approach that efficiently identifies biological activities in large chemical libraries. *Proc Natl Acad Sci USA* 2006; **103**:11473-11478.
70 Chen H, Liu L, Jones SA, *et al.* Selective inhibition of the west Nile virus methyltransferase by nucleoside analogs. *Antiviral Res* 2013; **97**:232-239.
71 Chen H, Zhou B, Brecher M, *et al.* S-adenosyl-homocysteine is a weakly bound inhibitor for a flaviviral methyltransferase. *PLoS One* 2013; **8**:e76900.
72 Zhang FC, Li XF, Deng YQ, Tong YG, Qin CF. Excretion of infectious Zika virus in urine. *Lancet Infect Dis* 2016; **16**:641-642.
73 Deng YQ, Zhang NN, Li CF, *et al*. Adenosine analog NITD008 is a potent inhibitor of Zika virus. *Open Forum Infect Dis* 2016; **3**:ofw175.
74 Sterling T, Irwin JJ. ZINC 15--ligand discovery for everyone. *J Chem Inf Model* 2015; **55**:2324-2337.

(**Supplementary information** is linked to the online version of the paper on the *Cell Research* website.)